frontiers in Ecology and Evolution

ORIGINAL RESEARCH
published: 17 March 2021
doi: 10.3389/fevo.2021.584325

Bioavailable Strontium, Human Paleogeography, and Migrations in the Southern Andes: A Machine Learning and GIS Approach

Ramiro Barberena[1,2], Marcelo Cardillo[3], Gustavo Lucero[4], Petrus J. le Roux[5]*, Augusto Tessone[6], Carina Llano[7], Alejandra Gasco[1,2], Erik J. Marsh[1], Amalia Nuevo-Delaunay[8], Paula Novellino[9], Cecilia Frigolé[1], Diego Winocur[10], Anahí Benítez[10], Luis Cornejo[11], Fernanda Falabella[12], Lorena Sanhueza[12], Francisca Santana Sagredo[13], Andrés Troncoso[12], Valeria Cortegoso[1,2], Víctor A. Durán[1,2] and César Méndez[8]**

[1] Laboratorio de Paleoecología Humana, Instituto Interdisciplinario de Ciencias Básicas (ICB), Consejo Nacional de Investigaciones Científicas y Técnicas (CONICET), Facultad de Ciencias Exactas y Naturales, Universidad Nacional de Cuyo, Mendoza, Argentina, [2] Facultad de Filosofía y Letras, Universidad Nacional de Cuyo, Mendoza, Argentina, [3] Instituto Multidisciplinario de Historia y Ciencias Humanas, Consejo Nacional de Investigaciones Científicas y Técnicas (CONICET), Ciudad Autónoma de Buenos Aires, Argentina, [4] Departamento de Antropología, Facultad de Ciencias Sociales y Humanidades, Universidad Católica de Temuco, Temuco, Chile, [5] Department of Geological Sciences, University of Cape Town, Cape Town, South Africa, [6] Instituto de Geocronología y Geología Isotópica, Universidad de Buenos Aires, Consejo Nacional de Investigaciones Científicas y Técnicas (CONICET), Ciudad Autónoma de Buenos Aires, Argentina, [7] Facultad de Ciencias Aplicadas a la Industria, Universidad Nacional de Cuyo, Consejo Nacional de Investigaciones Científicas y Técnicas (CONICET), San Rafael, Argentina, [8] Centro de Investigación en Ecosistemas de la Patagonia (CIEP), Coyhaique, Chile, [9] Museo de Ciencias Naturales y Antropológicas Juan C. Moyano, Consejo Nacional de Investigaciones Científicas y Técnicas (CONICET), Mendoza, Argentina, [10] Departamento de Ciencias Geológicas, Facultad de Ciencias Exactas y Naturales, Instituto de Estudios Andinos (IDEAN), Universidad de Buenos Aires, Ciudad Autónoma de Buenos Aires, Argentina, [11] Departamento de Antropología, Universidad Alberto Hurtado, Santiago, Chile, [12] Departamento de Antropología, Universidad de Chile, Santiago, Chile, [13] Pontificia Universidad Católica de Chile, Santiago, Chile

OPEN ACCESS

Edited by:
Clement Pierre Bataille, University of Ottawa, Canada

Reviewed by:
Omar Reyes, Universidad de Magallanes, Chile
Matthew Wooller, University of Alaska Fairbanks, United States

***Correspondence:**
Ramiro Barberena
rbarberena@mendoza-conicet.gob.ar
César Méndez
cesar.mendez@ciep.cl
Petrus J. le Roux
petrus.leroux@uct.ac.za

Specialty section:
This article was submitted to Paleoecology, a section of the journal Frontiers in Ecology and Evolution

Received: *16 July 2020*
Accepted: *12 February 2021*
Published: *17 March 2021*

Citation:
Barberena R, Cardillo M, Lucero G, le Roux PJ, Tessone A, Llano C, Gasco A, Marsh EJ, Nuevo-Delaunay A, Novellino P, Frigolé C, Winocur D, Benítez A, Cornejo L, Falabella F, Sanhueza L, Santana Sagredo F, Troncoso A, Cortegoso V, Durán VA and Méndez C (2021) Bioavailable Strontium, Human Paleogeography, and Migrations in the Southern Andes: A Machine Learning and GIS Approach. Front. Ecol. Evol. 9:584325. doi: 10.3389/fevo.2021.584325

The Andes are a unique geological and biogeographic feature of South America. From the perspective of human geography, this mountain range provides ready access to highly diverse altitudinally arranged ecosystems. The combination of a geologically and ecologically diverse landscape provides an exceptional context to explore the potential of strontium isotopes to track the movements of people and the conveyance of material culture. Here we develop an isotopic landscape of bioavailable strontium (87Sr/86Sr) that is applied to reconstruct human paleogeography across time in the southern Andes of Argentina and Chile (31°–34°S). These results come from a macro-regional sampling of rodents (N = 65) and plants (N = 26) from modern and archeological contexts. This "Southern Andean Strontium Transect" extends over 350 km across the Andes, encompassing the main geological provinces between the Pacific coast (Chile) and the eastern lowlands (Argentina). We follow a recently developed approach to isoscape construction based on Random Forest regression and GIS analysis. Our results suggest that bioavailable strontium is tightly linked with bedrock geology and offers a highly resolved proxy to track human paleogeography involving the levels of territories or daily mobility and anomalous events that disrupt home ranges, such as migration. The

southern Andes provide an ideal geological setting to develop this approach, since the geological variation in rock age and composition produces distinctive isotopic signatures for each main biogeographical region. Finally, we apply this framework to a set of results from human remains from the Uspallata Valley in Mendoza (Argentina), to assess the incidence of migration in the key period of the consolidation of agropastoral economies between AD 800 and 1400. The application of the isoscape to the values from human remains confirms the persistence of human groups with relatively restricted territories encompassing Uspallata and the adjacent Precordillera between AD 800 and 1500. We also identify a pulse of human migration between AD 1280 and 1420, shortly preceding the Inka conquest. Looking forward, we expect to converge with ongoing efforts in South America to build a continental research framework to track the movement of people, animals, and artifacts across space and time.

Keywords: bioavailable strontium, archeology, Andes, machine learning, human paleomobility, migrations, radiogenic strontium isotope

INTRODUCTION

Strontium isotopes ($^{87}Sr/^{86}Sr$) in human teeth and bone remains average the biologically available strontium in the landscape(s) inhabited in the past (Price et al., 2002; Bentley, 2006), providing a proxy of the geographic place of origin of an individual and the spatial scale of the territories occupied (Price et al., 2000; Montgomery, 2010; Knudson et al., 2014a; Laffoon et al., 2017). Since first applied in archeology (Ericson, 1985), strontium isotopes ($^{87}Sr/^{86}Sr$) have widened the scope of archeological enquiry across analytical scales, from small-scale aspects of human life-history and identity construction (Kutschera and Müller, 2003; Montgomery, 2010; Andrushko et al., 2011; Knudson et al., 2012; Torres-Rouff and Knudson, 2017) to large-scale group migration processes (Borić and Price, 2013; Yu et al., 2020). In addition, convergent interdisciplinary efforts from geology, ecology, paleoecology, forensics, and archeology have resulted in increasingly more sophisticated approaches to assess the mobility of the organisms under study and, building on this, to identify non-local residence and migration on different spatial and social scales (Price et al., 2002; Bentley, 2006; Montgomery et al., 2007; Bataille et al., 2014, 2020; Kootker et al., 2016; Tipple et al., 2018; Willmes et al., 2018; Scaffidi and Knudson, 2020; Snoeck et al., 2020). Thus, resulting from the combination of growing frames of scientific enquiry, robust methodological approaches, and extensive databases, we consider it is fair to describe the present time as a "golden age" of strontium isotopes to geographically source materials across space and time. However, this advance is highly heterogeneous in the different continents (Bataille et al., 2020). In South America, strontium isotopic research has been largely focused in the Central and South-Central Andes encompassing Peru, western Bolivia and northern Chile (Knudson et al., 2014a,b; Dantas and Knudson, 2016; Chala-Aldana et al., 2018; Mader et al., 2018; Slovak et al., 2018; Standen et al., 2018; Takigami et al., 2019; Santana-Sagredo et al., 2021). We have recently started a project with the goal of extending the bioavailable strontium framework to the southern Andes in Central Argentina and Chile (Barberena et al., 2017, 2019, 2020; Durán V. et al., 2018). From a comparative perspective, this project allows incorporating Andean regions with different archeological trajectories of socio-economic change, complexity, and possibly diverse incidence of migrations compared to the more systematically studied Central Andes.

The general objective of this project is to develop a multidisciplinary approach to human scale of mobility, role of migration, and trans-Andean interaction since the initial human peopling in the Pleistocene-Holocene transition (García, 2003), with a focus on the period witnessing the evolution of agropastoral economies in the last 2,000 years (Gil et al., 2014; Falabella et al., 2016; Llano et al., 2017; Durán V. et al., 2018; Gasco, 2018). In this agenda, the specific goal of this paper is to present the strontium isotope ($^{87}Sr/^{86}Sr$) results for plant and rodent samples from a trans-Andean transect encompassing from the Pacific Ocean in Central Chile to the eastern lowlands in Argentina (31°–34°S) (**Figure 1**). The "Southern Andean Strontium Transect" (SAST, from now onward) samples the main geological provinces across the Andes that span the last ca. 450 my, between the lower Paleozoic and the late Quaternary. From a methodological perspective, we apply an innovative and robust approach based on Random Forest regression designed to assess which biophysical variables predict the observed strontium isotope variation with the highest resolution (Bataille et al., 2014, 2018, 2020; see also Serna et al., 2020). Our results demonstrate that the southern Andes provide an ideal geological setting for the development of this approach, since there is an impressive geological variation in rock age and composition that produces distinctive isotopic signatures for each biogeographical region of archeological relevance. Finally, we apply this geostatistical framework to a recently published archeological case-study from the Uspallata montane Valley in northwestern Mendoza, Argentina (**Figure 1**). The specific archeological goal consists in assessing the spatial scale of mobility of human remains buried in five archeological cemeteries spanning the key period between the consolidation of agropastoral economies and the regional conquest by the Inka

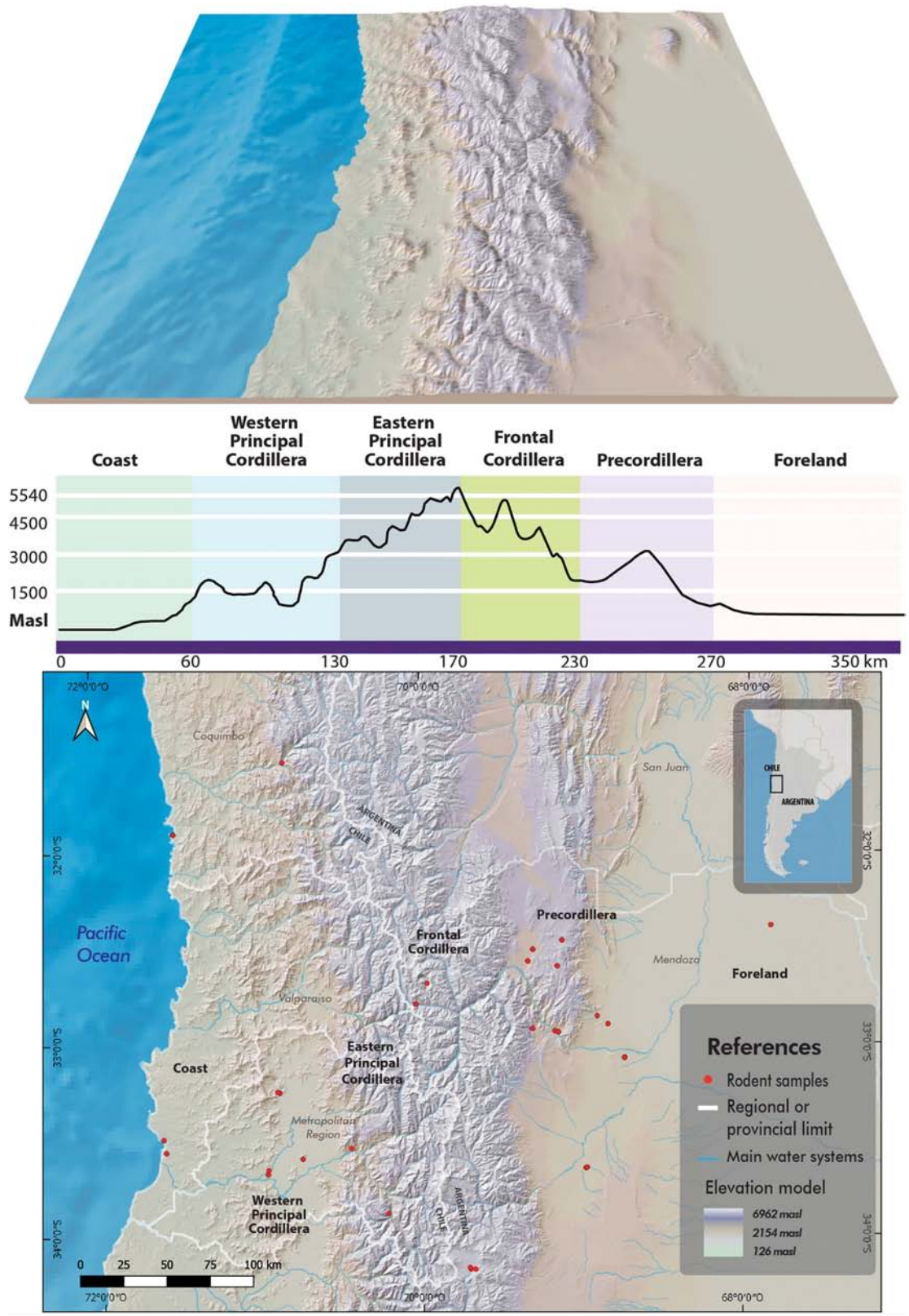

FIGURE 1 | Study area and location of the samples for isotopic analysis.

Empire (AD 800–1400) (Barberena et al., 2020). Building on this, we assess the incidence of migration in the conformation of these human groups through time.

GEOLOGICAL, ECOLOGICAL, AND ARCHEOLOGICAL BACKGROUND

Geological Framework for the Analysis of Bioavailable Strontium

The southern Andes of Argentina and Chile is a mountain belt formed at the convergent margin between the Nazca and South American plates. Our study area encompasses Central Argentina and Chile and is located in the transition zone between the Pampean flat slab, characterized by a shallow subduction angle resulting in a volcanic gap, and the normal subduction zone of central Chile and Argentina (Ramos and Folguera, 2009). This segment corresponds to the northernmost active volcanism of the Southern Volcanic Zone of the Andean belt. In this latitudinal block, the Andes are composed of seven major morpho-structural provinces that provide our framework for the sampling and analysis of bioavailable strontium. Since it represents a particular strontium biozone in terms of human diet and mobility (Banner, 2004; Standen et al., 2018), we also include the Pacific Ocean as the first unit along the west to east SAST, as follows: (1) Pacific Ocean; (2) Coastal Cordillera; (3) Central Depression-Central Chilean Valley; (4) Western Principal Cordillera; (5) Eastern Principal Cordillera; (6) Frontal Cordillera; (7) Precordillera; and (8) Active Foreland or Quaternary lowlands (**Figure 2**).

The first unit is the (1) *Pacific Ocean* that was sampled in coastal settings between the modern towns of Los Vilos in the north (31°55′S) and San Antonio in the south (33°40′S) (**Figure 1**). Eastwards from the Pacific coast follows the *Coastal Cordillera* (2), which has a Paleozoic-Triassic basement in the west and Jurassic-Cretaceous clastic and volcanoclastic intra-arc sequences in the east. These units are intruded by Upper Cretaceous igneous rocks of dioritic to monzodioritic composition. The *Central Depression* (3) is an extensional basin developed since late Eocene-Oligocene times and filled by volcanic and volcanoclastic rocks (Charrier et al., 2002). During the early to mid-Miocene, calc-alkaline andesitic lava, and acid pyroclastic flows of the Farellones Formation were deposited in the central part of the basin (Kurtz et al., 1997). From the eastern flank of the Central Depression develops the *Cordillera Principal*, divided into two geological provinces with different rock ages and compositions: the *Western Cordillera Principal* (4), formed by Oligocene and Miocene volcanic and intrusive rocks, and the *Eastern Cordillera Principal* (5), constituted by sedimentary Mesozoic rocks deformed into the Aconcagua fold and thrust belt (Giambiagi et al., 2009). The Jurassic to middle Cretaceous sedimentary rocks of the Eastern Cordillera Principal include marine evaporites, sandstones, clay-stones, and limestones. Immediately eastwards lies the *Cordillera Frontal* (6), containing a Paleozoic basement constituted by sedimentary, metamorphic and igneous rocks intruded by Upper Paleozoic granitoids unconformably covered by Permo-Triassic igneous rocks. The *Precordillera* unit (7) is emplaced eastwards of the Cordillera Frontal and has a southern limit at ∼33°S. It is composed of Lower and Upper Paleozoic (Cambrian to Permian) sedimentary rocks intruded by Paleozoic calc-alkaline granitoids (Furque and Cuerda, 1979; Astini et al., 1995; Giambiagi et al., 2003). Finally, late Quaternary clastic deposits occur in the *Active Foreland* (8), to the east of the Frontal Cordillera and Precordillera. This foreland basin results from the progressive erosion of the rocks forming the different morpho-structural Andean units. Synthesizing these trends, rock age increases eastwards from the Pacific coast, hence leading to low $^{87}Sr/^{86}Sr$ in the west and increasingly higher values eastwards (Barberena et al., 2017).

Ecology Across the Southern Andean Strontium Transect

This latitudinal band of the Andes presents the highest average altitude separating the Pacific and Atlantic slopes of South America (Clapperton, 1993). The interaction between the Andean topography and the prevailing westerly storm tracks bringing humidity to the continent from the Pacific Ocean produces marked spatial variation in temperature, precipitation, and ecology (Garreaud, 2009; Oyarzabal et al., 2018; Masiokas et al., 2020). These communities are dominated by shrubs in the lowlands and by an increase in the herbaceous stratum up to 3,300 masl (Muñoz-Schick et al., 2000). There is a succession of vegetation communities by altitude (from east to west): open scrubland (1,000–1,500 masl), sub-Andean and Andean scrubland (1,500–2,700 masl), Andean steppe (2,700–3,300 masl), and Andean desert (>3,300 masl). Andean steppe and scrubland associated with the Patagonia phytogeographical province (3,300–1,400 masl) are followed to the east by the dry scrublands of the Monte phytogeographical province (Abraham et al., 2009).

The Andean highlands are characterized by large amounts of precipitation occurring mostly during winter as snow and, as altitude decreases, ecosystems become increasingly dry east and westwards. In this geographical context, the SAST between the Pacific Ocean and the eastern Andean lowlands connects a succession of tightly packed altitudinally arranged ecosystems (**Figure 3**). This is a highly seasonal landscape where large areas above 2,500 masl would only be available for systematic occupation and circulation during the summer months (Durán V. et al., 2018). This is a fundamental landscape feature that would have conditioned patterns of trans-Andean human movement and social interaction (Cornejo and Sanhueza, 2011; Cortegoso et al., 2016).

Archeological Background

The archeological record from the southern Andes provides a window to study diachronic socio-demographic processes spanning the early human dispersion and colonization of the continent beginning in the late Pleistocene, the effective occupation of available spaces within socially defined territories, processes of economic intensification and reduction of mobility, development of agropastoral economies, and socio-political complexity ending with the successive annexation by the Inka

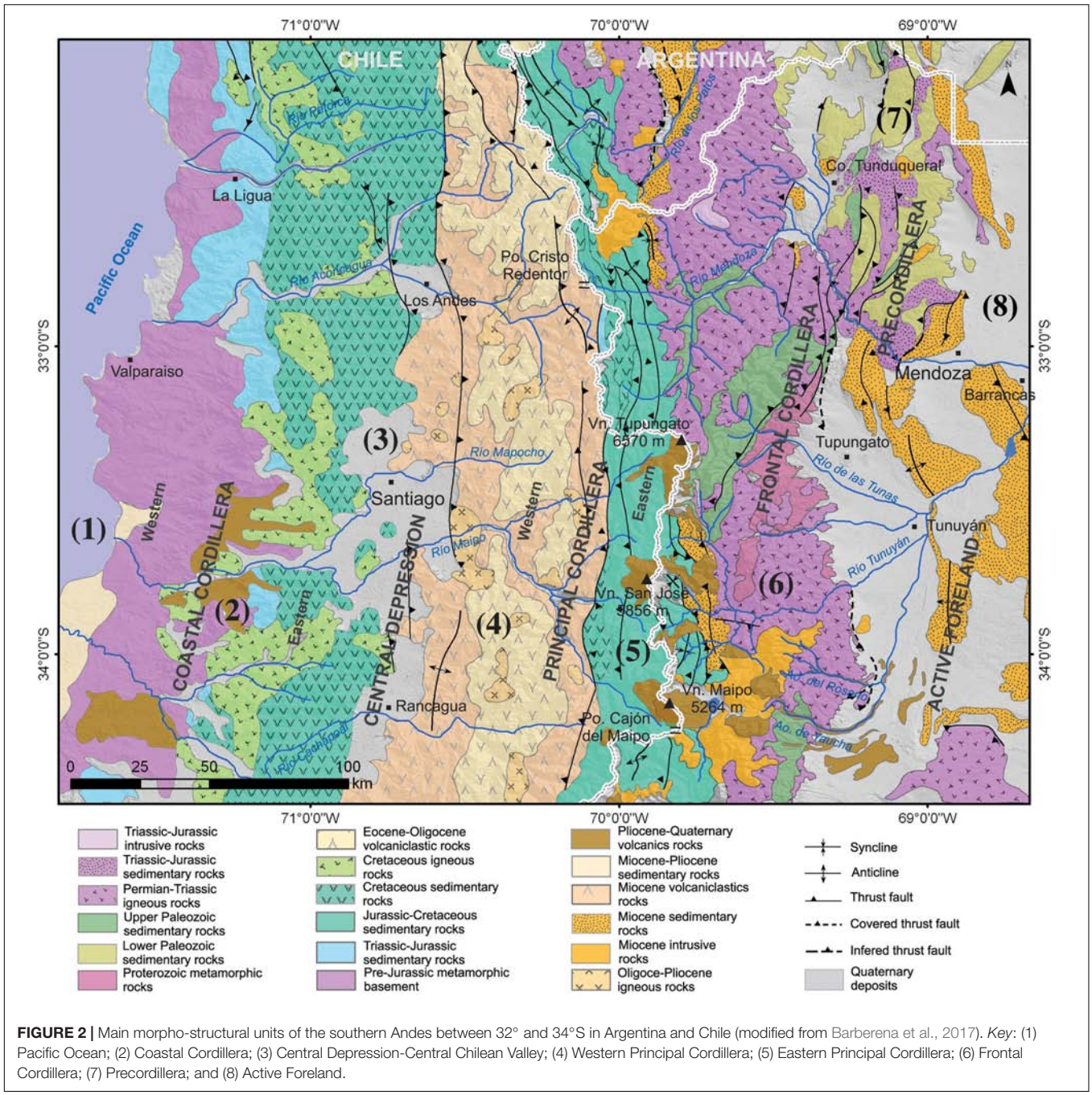

FIGURE 2 | Main morpho-structural units of the southern Andes between 32° and 34°S in Argentina and Chile (modified from Barberena et al., 2017). *Key*: (1) Pacific Ocean; (2) Coastal Cordillera; (3) Central Depression-Central Chilean Valley; (4) Western Principal Cordillera; (5) Eastern Principal Cordillera; (6) Frontal Cordillera; (7) Precordillera; and (8) Active Foreland.

and Spanish empires. The scale(s) of human paleomobility and the role of migration through time would have been key components of the trajectories of these and other historical processes.

Humans have occupied the coastal and mountain environments of the southern Andes of Argentina and Chile since the late Pleistocene (García, 2003; Méndez Melgar, 2013; Méndez et al., 2018). For most of the Holocene, mobile foraging was the dominant way of life, documented by a variety of hunting weapon systems, the consumption of diverse plant taxa such as algarrobo (*Prosopis* sp.) and molle (*Schinus polygamus*), and the wild camelid guanaco as some of the main staples (Bárcena, 2001; Llano, 2015; Cornejo et al., 2016). There are indications of a major regional shift in human adaptations and economic practices starting before 2,000 years BP. Domestic plants are recorded, including maize (*Zea mays*), quinoa (*Chenopodium quinoa*), beans (*Phaseolus* sp.), and squash (*Cucurbita* sp.) (Planella et al., 2015; Llano et al., 2017), as well as the earliest pottery (Sanhueza and Falabella, 1999; Marsh, 2017). Burial practices became more elaborate and some of the first formal cemeteries in central-western Argentina are dated to these centuries (Rusconi, 1962; Novellino et al., 2013; Menéndez et al.,

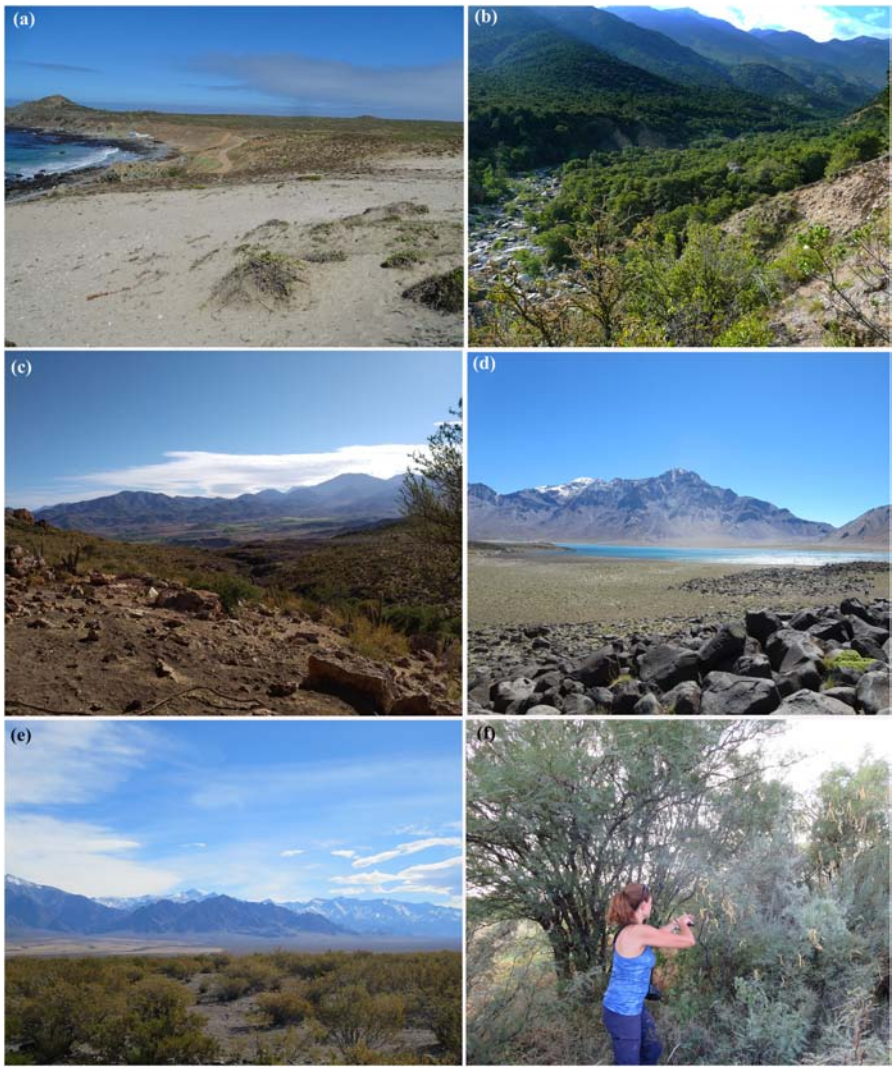

FIGURE 3 | Main regions incorporated in the Southern Andean Transect. *Key*: **(a)** Bahía La Cachina, Pacific Coast (Chile). **(b)** El Manzano, Western Cordillera Principal (Chile). **(c)** Cogotí, Western Cordillera Principal (Chile). **(d)** Laguna del Diamante, Eastern Principal Cordillera (Argentina). **(e)** Uspallata Valley, transition between Frontal Cordillera and Precordillera (Argentina). **(f)** Corsemar, Active Foreland (Argentina).

2014). The llama domestic camelid (*Lama glama*) would have been present in areas within this region (Gasco, 2018). For at least a millennium, people had an agropastoral lifeway that would have combined hunting, gathering, farming, and herding in diverse proportions. The Inka Empire arrived in central Argentina and Chile immediately after AD 1400 (Cornejo, 2014; Marsh et al., 2017).

MATERIALS AND METHODS

Sampling Strategy

The SAST extends for over 350 km between the Pacific Ocean (Chile) and the eastern lowlands in Mendoza Province (Argentina) (**Figure 1**). In order to build an isoscape of bioavailable strontium across the southern Andes we sampled small rodents—with restricted home ranges—and plants (Price et al., 2002; Copeland et al., 2016; Snoeck et al., 2018; Scaffidi and Knudson, 2020). Our strategy was initially designed to target rodents as the main proxy for bioavailable strontium (Barberena et al., 2017), and we turned to plant samples for areas where rodent samples were not readily available. Accordingly, the sampling was not designed to formally compare these two substrates. However, since we detected important differences for rodents and plants coming from some of the geological regions, we develop two alternative Random Forest models, respectively, analyzing rodents, on the one hand, and rodents and plants, on the other hand. We then explore the robustness of the resulting models and the main biophysical variables that explain the observed isotopic variation.

The rodent samples include modern and archeological specimens (Barberena et al., 2019, 2020) and the plant samples

are all modern. Two strategies for sampling plants were applied: the plant samples from Argentina combine five near-located individuals from the same species in each sampling locality and the samples from Chile correspond to only one plant in each case. It is not expected that this may cause any significant difference in the results obtained. Whenever possible, native taxa were selected (**Table 2**). Considering the wide altitudinal (∼0–3,400 masl), climatic, and ecological variation in the SAST, three different plant types were sampled: in the Monte of the dry lowlands of eastern Argentina we sampled shrubs such as *Larrea, Prosopis, Schinus,* and *Adesmia*, with deep rooting systems reaching the groundwater at beyond 20 m-depth; in the dry highlands of the Patagonian phytogeographical Province we selected grasses (Poaceae) with low-depth root systems; and finally in the more mesic lowland settings west of the Andes we sampled evergreen trees (*Quillaja saponaria, Peumus boldus, Eucalyptus robusta*), where a large part of the roots providing the soil nutrients are located near the surface (Díaz et al., 1999; Jobbágy et al., 2011). Considering that plant physiology conditions the sources of strontium uptake within the same landscape (Capo et al., 1998; English et al., 2001; Reynolds et al., 2012; Grimstead et al., 2017), we will augment our current sampling in order to account for possible inter-specific differences within geological regions.

The geological provinces described above were used as the units of analysis for the bioavailable strontium sampling. However, the samples are not randomly distributed within these regions since in many cases work focused in areas of archeological interest, such as Los Vilos, Combarbalá, and the Maipo River in Chile and the Uspallata Valley and Laguna del Diamante in Argentina. However, these are representative of the geologic areas from which the samples were gathered. The plant and rodent samples are distributed in the spatial units of analysis as follows: Pacific coast, $n = 15$; Coastal Cordillera, $n = 10$; Western Principal Cordillera, $n = 10$; Eastern Principal Cordillera, $n = 10$; Frontal Cordillera $n = 8$; Precordillera, $n = 24$; and Active Foreland, $n = 14$.

Laboratory Methods

Strontium isotope analysis was performed in the Department of Geological Sciences, University of Cape Town, following routine chemical and MC-ICP-MS methods (Copeland et al., 2010, 2016; Scott et al., 2020). Plant sample material was cut into <1 cm pieces and subsamples of plants from each sampling locality where placed in a pure quartz silica crucible. The crucibles were placed in a muffle furnace set at 300°C, and the temperature ramped by 100°C/h to 650°C and held at that temperature overnight. Once cooled, the ashed plant material was transferred to a 7 ml Savillex Teflon beaker. For digestion, 2 ml of a 4:1 mixture of 48% HF: 65% HNO_3 was added, the beaker closed and placed overnight on a hotplate set at 140°C. Following two stages of dry down and re-dissolving in 1 ml 65% HNO_3, 1.5 ml 2 M HNO_3 was added and allowed to settle overnight to be ready for strontium separation chemistry. Powdered bone and enamel samples were weighed into 7 ml Savillex Teflon beakers, 2–3 ml of 65% HNO_3 added and the closed beakers placed on a hotplate at 140°C for an hour. Following complete sample dissolution, the beakers were opened, and the samples dried. Once dry, the samples were redissolved in 1.5 ml 2 M HNO_3 to be for strontium separation chemistry.

Strontium separation chemistry for all samples followed the same method (Pin et al., 1994) and used Triskem Sr. Spec resin. The separated strontium fraction for each sample was dried down, dissolved in 2 ml 0.2% HNO_3 and diluted to 200 ppb Sr concentrations for Sr isotope ratio analysis using a Nu Instruments NuPlasma HR MC-ICP-MS. Analyses were referenced to bracketing analyses of NIST SRM987, using a $^{87}Sr/^{86}Sr$ reference value of 0.710255. All strontium isotope data are corrected for isobaric rubidium interference at 87 amu using the measured signal for ^{85}Rb and the natural $^{85}Rb/^{87}Rb$ ratio. Instrumental mass fractionation was corrected using the measured $^{86}Sr/^{88}Sr$ ratio, the exponential law, and an accepted $^{86}Sr/^{88}Sr$ value of 0.1194. An in-house carbonate reference material processed and measured with the batches of unknown samples in this study yielded results ($^{87}Sr/^{86}Sr$ 0.708914 ± 0.000045 2σ; $n = 12$) in agreement with long-term results for this reference material from this facility ($^{87}Sr/^{86}Sr$ 0.708911 ± 0.000040 2σ; $n = 414$). Total procedural blanks processed with these samples yielded background Sr levels <250 pg, and therefore negligible.

Random Forest, GIS, and Strontium Isoscapes

The Random Forest approach is based in a bootstrapping procedure that generates an ensemble (or forest) of trees resulting in different combinations of the target variable ($^{87}Sr/^{86}Sr$) and its biophysical predictors (Breiman, 2001; Bataille et al., 2018). Compared to other classification or regression methods, the average of the Random Forest trees has smaller variance and a higher predictive performance. In addition, compared with other machine learning methods it is less prone to overfitting (Kuhn, 2013). As has been robustly demonstrated (Bataille et al., 2018, 2020), this method allows combining quantitative and categorical variables and has a remarkable versatility to generate $^{87}Sr/^{86}Sr$ isoscapes.

In order to determine the most parsimonious subset of variables with the highest predictive power, the Variable Selection using Random Forest (VSURF) package was used (Genuer et al., 2019). We incorporate spatial, geological, and bioclimatic variables in the model (**Table 1**). We also utilize as a predictor variable the "bedrock model" (Bataille et al., 2018, 2020) that predicts the median, Quartile 1 and Quartile 3 of $^{87}Sr/^{86}Sr$ values for bedrock in a global scale. This will expand the recent application developed by Serna et al. (2020) for northern Patagonia. The variables are introduced in a stepwise manner in order to detect the combination of predictors that reduces the mean "Out-of-Bag Error" (see details in **Supplementary Data**).

The Random Forest approach divides the total isotopic sample into a *training phase* of the model, encompassing 80% ($n = 72$) of the results, while the remaining 20% ($n = 19$) was used in a *testing phase* to assess the predictive capacity of new data of the model produced (see script in **Supplementary Material**).

TABLE 1 | List of locational, geological, and bioclimatic variables used in the model.

Name	Variable	Type	Scale	Source
Latitude	Latitude	C	90 m	
Longitude	Longitude	C	90 m	
r.elevation	Altitude (SRTM masl)	C	90 m	Jarvis et al., 2008
Distance	Distance to the nearest coast	C		
Geological province	Geological region	D		Barberena et al., 2017
r.m1	Median bedrock model	D	1 km	Bataille et al., 2020
Glim_UTM	Lithological classification	D	1 km	Hartmann and Moosdorf, 2012
r.meanage_geol	GLiM age attribute (Myrs)	D	1 km	Hartmann and Moosdorf, 2012
r.clay	Clay (weight%)	C	250 m	Hengl et al., 2017
r.pH	Soil pH in H_2O solution	C	250 m	Hengl et al., 2017
r.dust.t	Multi-models average	C	1° × 1°	Mahowald et al., 2006
r.salt.t	CCSM.3 simulation	C	1.4° × 1.4°	Hengl et al., 2017
Vapr_01	Evapotranspiration January (kPa)	C	30 arc s	Fick and Hijmans, 2017
Vapr_07	Evapotranspiration July (kPa)	C	30 arc s	Fick and Hijmans, 2017
Bio15	Seasonality based on temperature	C	30 arc s	Fick and Hijmans, 2017
Bio4	Seasonality based on precipitation	C	30 arc s	Fick and Hijmans, 2017
Prec_01	Precipitation January (mm)	C	30 arc s	Fick and Hijmans, 2017
Prec_07	Precipitation July (mm)	C	30 arc s	Fick and Hijmans, 2017
Tavg_01	Average temperature January (°C)	C	30 arc s	Fick and Hijmans, 2017
Tavg_07	Average temperature July (°C)	C	30 arc s	Fick and Hijmans, 2017
Tmax_01	Maximum temperature January (°C)	C	30 arc s	Fick and Hijmans, 2017
Tmax_07	Maximum temperature July (°C)	C	30 arc s	Fick and Hijmans, 2017
Tmin_01	Minimum temperature January (°C)	C	30 arc s	Fick and Hijmans, 2017
Tmin_07	Minimum temperature July (°C)	C	30 arc s	Fick and Hijmans, 2017
wc2 1_5m_01	Evapo-transpiration January (kPA)	C	30 arc s	Fick and Hijmans, 2017
wc2 1_5m_07	Evapo-transpiration July (kPA)	C	30 arc s	Fick and Hijmans, 2017

C, continuous; D, discrete.

The full dataset is first randomized to avoid any structure resulting from record or sampling order. The Random Forest was first passed through a tuning phase in order to find the optimal number of variable combinations with respect to the Out-of-Bag error estimate, by using only the subset of variables automatically selected by VSURF. Afterward, we selected the model showing the smaller Mean Squared Error (MSE) between predicted and observed $^{87}Sr/^{86}Sr$ values. The relative weight of each variable in reducing the overall error in the Random Forest model was measured by the "variable importance impurity measure," graphically represented by the partial dependence of $^{87}Sr/^{86}Sr$ values on those variables. The $^{87}Sr/^{86}Sr$ values predicted by the Random Forest model in relation to the predictor variables were then used to produce the isoscapes, while the residuals between the predicted and observed values provide the uncertainty associated with the isoscape. In addition, the uncertainty in the prediction for each case was measured using the standard error generated by the data used to generate the model. Finally, we used a Mantel correlogram (Legendre and Fortin, 1989) to assess the existence of remaining spatial structuration in the $^{87}Sr/^{86}Sr$ values unaccounted for by the covariables of the model, that would indicate that unknown variables have a weight in structuring the observed variation. To accomplish this, we utilized the residuals of the Random Forest model with 10,000 permutations on two distance-matrices produced on the basis of the residuals and the spatial coordinates on the training model (80% of the sample).

The Random Forest model was adjusted with the software Ranger (Wright and Ziegler, 2017) and tuneRanger (Probst et al., 2019) that implement quantile regression for Random Forest, and with VSURF (Genuer et al., 2019). The graphs of partial dependence were produced with the pdp package (Greenwell, 2017) and the analysis of spatial structure in the residuals was conducted with the packages ncf (Bjornstad and Cai, 2020) and ecodist (Goslee and Urban, 2007). All the analyses were performed in R Core Team (2020). For the geostatistical analysis, we compiled a georeferenced database incorporating the results of the Random Forest model. This information was processed in the platform QGIS 3.14 in order to build the isoscapes of bioavailable strontium using the Inverse Distance Weighing—IDW—function (Kootker et al., 2016; Bataille et al., 2018).

RESULTS

Strontium Isotopes in Plant and Rodent Samples

We present new $^{87}Sr/^{86}Sr$ results for modern plant samples ($n = 26$) (**Table 2**), which are combined with previously published

TABLE 2 | $^{87}Sr/^{86}Sr$ results for plant samples from the southern Andes of Argentina and Chile (source: this paper).

Sampling site	Geological province	Taxon	Latitude (S)	Longitude (W)	$^{87}Sr/^{86}Sr$	±2s
Cartagena Bay	Pacific Coast	*Quillaja saponaria* (native)	33°30.451′	71°36.411′	0.708132	0.000012
Rocas de Santo Domingo	Pacific Coast	Unknown	33°37.903′	71°38.058′	0.707697	0.000012
Cartagena	Coastal Cordillera	Unknown	33°33.037′	71°33.987′	0.705779	0.000014
El Membrillo	Coastal Cordillera	*Eucalyptus robusta* (non-native)	33°28.569′	71°36.265′	0.707543	0.000012
Malvilla	Coastal Cordillera	*Acacia caven* (native)	33°34.823′	71°30.224′	0.706011	0.000014
Las Palmas	Coastal Cordillera	Unknown	33°37.204′	71°25.091′	0.705627	0.000013
Puangue	Coastal Cordillera	*Eucalyptus robusta* (non-native)	33°38.620′	71°21.936′	0.705894	0.000013
Yeso River	W Principal C.	*Peumus boldus* (native)	33°43.848′	70°8.341′	0.704203	0.000012
Maipo River	W Principal C.	*Peumus boldus* (native)	33°46.530′	70°15.562′	0.705419	0.000016
Maipo River	W Principal C.	*Quillaja saponaria* (native)	33°34.906′	70°'24.093′	0.705654	0.000014
La Reina	W Principal C.	*Ligustrum lucidum* (non-native)	33°26.946′	70°31.640′	0.704452	0.000011
Yeso River	E Principal Cordillera	Unknown	33°37.330′	69°57.770′	0.70665	0.000028
Laguna del Diamante	E Principal Cordillera	Poaceae (native)	34°10.802′	69°39.502′	0.705656	0.000011
Paramillos Ignimbrite	Frontal Cordillera	*Schinus* spp. (native)	34°14.951′	69°19.411′	0.706885	0.000016
Road to Laguna del Diamante	Frontal Cordillera	*Adesmia* sp. (native)	34°13.456′	69°25.874′	0.711841	0.000010
Cerro Tunduqueral	Precordillera	*Prosopis* aff. *Alpataco* (native)	32°31.967′	69°18.572′	0.706689	0.000012
Cerro Tunduqueral	Precordillera	*Larrea cuneifolia* (native)	32°31.970′	69°18.468′	0.706818	0.000014
San Alberto-Tambillos	Precordillera	*Larrea nitida* (native)	32°23.772′	69°23.398′	0.707777	0.000014
San Alberto-Tambillos	Precordillera	*Larrea divaricata* (native)	32°23.911′	69°23.595′	0.707598	0.000013
Uspallata-Usina Sur	Precordillera	*Larrea nitida* (native)	32°38.055′	69°22.467′	0.70754	0.000008
Uspallata-Usina Sur	Precordillera	*Fabiana denudata* (native)	32°37.951′	69°22.541′	0.707014	0.000012
Paramillos	Precordillera	*Larrea nitida* (native)	32°28.518′	69°11.593	0.707572	0.000010
Road to Canota	Precordillera	*Mulinum spinosum* (native)	32°30.740′	69°2.845′	0.707747	0.000014
Cruz de Paramillos	Precordillera	Poaceae (native)	32°29.592′	69°7.050′	0.70815	0.000011
Pampa de Canota	Precordillera	Poaceae (native)	32°38.427′	69°8.081′	0.707834	0.000013
Corsemar	Active Foreland	*Larrea cuneifolia* (native)	32°40.241′	68°52.860′	0.707036	0.000015

results for rodent samples (n = 65) (**Table 3**). While this sample can be considered as preliminary given the large size of the study-area, the results offer a first characterization of the geological provinces across the southern Andes.

The $^{87}Sr/^{86}Sr$ values are normally distributed (W = 0.98094, p = 0.2039) ranging between 0.70393 and 0.71184 with an average of 0.70723 ± 0.00177. When considering the plant and rodent samples separately, the 26 plant samples have a mean $^{87}Sr/^{86}Sr$ value of 0.70689 ± 0.00149, a maximum value of 0.71184 (Frontal Cordillera), and a minimum value of 0.7042 (Western Principal Cordillera). The 65 rodent samples have a mean $^{87}Sr/^{86}Sr$ value of 0.70736 ± 0.00187, a maximum value of 0.7109 (Precordillera), and a minimum value of 0.70393 (Western Principal Cordillera).

Particularly for the Precordillera geological province, that includes the key archeological locality of the Uspallata Valley discussed here (**Figure 1**), we have adequate sample sizes for plant and rodent samples to allow a first comparison. Unexpectedly, the respective isotopic ranges do not overlap. Plants have a mean value of 0.70747 ± 0.00047 and rodents of 0.70964 ± 0.00082. Interestingly, not only rodents but also wild herbivore camelids from Uspallata-Precordillera fail to reproduce the signal for modern plants (Barberena et al., 2019). While this sampling was not designed to compare the performance of different substrates to build strontium isoscapes, these differences are considered large and they would have implications for the reconstruction of human paleomobility and migration. Accordingly, we explore next if there are differences in the main predictor variables of $^{87}Sr/^{86}Sr$ values in two alternative Random Forest models: one combining values for plants and rodents (n = 91) and another one including only rodents (n = 65). Based on this comparison we assess the predictive capacity of the two alternative models.

Random Forest Modeling and Strontium Isoscape

In the "Plants + Rodents" dataset, the selected Random Forest model explains a 76% of the variation in the observed OOB values with an MSE of 0.00000008 ($^{87}Sr/^{86}Sr$ RMSE = 0.0003), suggesting a good power of the predictive variables utilized and a low error. The variables with the highest predictive power are—in decreasing order of importance—Geological Province, Bio15 (temperature seasonality), and Mean-age, with a subordinate role by six other bioclimatic variables (**Figure 4A**). In the case of the "Rodents" sample, the selected Random Forest model accounts for 85% of the observed values with an OOB MSE = 0.0000007 ($^{87}Sr/^{86}Sr$ RMSE = 0.0007). The variables with a high predictive power are only three: Geological Province, Mean-age, and Distance to coast (**Figure 4B**). In sum, the "Rodents" model has a higher predictive capacity than the "Plants + Rodents" model (85 vs. 76%). Additionally, in the "Rodent" model this variation is accounted for by only three predictor variables, two of which are tightly connected with the geological substrate

TABLE 3 | $^{87}Sr/^{86}Sr$ results for rodent samples from the southern Andes (Argentina and Chile).

N	Site	Geological unit	Taxon	Latitude (S)	Longitude (W)	$^{87}Sr/^{86}Sr$	Source
1	Los Vilos	Pacific Coast	Rodentia	31°54.692′	71°30.616′	0.708395	Barberena et al., 2020
2	Los Vilos	Pacific Coast	Rodentia	31°54.692′	71°30.616′	0.708706	Barberena et al., 2020
3	Los Vilos	Pacific Coast	Rodentia	31°54.692′	71°30.616′	0.709022	Barberena et al., 2020
4	Los Vilos	Pacific Coast	Rodentia	31°54.692′	71°30.616′	0.708593	Barberena et al., 2020
5	Los Vilos	Pacific Coast	Rodentia	31°54.692′	71°30.616′	0.708885	Barberena et al., 2020
6	Los Vilos	Pacific Coast	Rodentia	31°54.692′	71°30.616′	0.708999	Barberena et al., 2020
7	Los Vilos	Pacific Coast	Rodentia	31°54.692′	71°30.616′	0.708898	Barberena et al., 2020
8	Los Vilos	Pacific Coast	Rodentia	31°54.692′	71°30.616′	0.709019	Barberena et al., 2020
9	LEP-C	Pacific Coast	*Myocastor coipus*	33°30.222′	71°36.580′	0.708572	Barberena et al., 2020
10	LEP-C	Pacific Coast	*Octodon* sp.	33°30.222′	71°36.580′	0.708197	Barberena et al., 2020
11	LEP-C	Pacific Coast	*Octodon* sp.	33°30.222′	71°36.580′	0.708566	Barberena et al., 2020
12	Arévalo 2	Pacific Coast	*Octodon* sp.	33°34.305′	71°35.675′	0.707365	Barberena et al., 2020
13	Arévalo 2	Pacific Coast	*Octodon* sp.	33°34.305′	71°35.675′	0.707754	Barberena et al., 2020
14	RML-015	Coastal Cordillera	*Octodon* sp.	33°16.154′	70°52.995′	0.704151	Barberena et al., 2020
15	E-101-3	Coastal Cordillera	Rodentia	33°41.661′	70°57.884′	0.706320	Barberena et al., 2020
16	RML-008	Coastal Cordillera	*Octodon* sp.	33°15.852′	70°53.816′	0.704150	Barberena et al., 2020
17	Cerro Chena	Coastal Cordillera	*Myocastor coipus*	33°36.926′	70°44.814′	0.705305	Barberena et al., 2020
18	E-101-1	Coastal Cordillera	*Myocastor coipus*	33°40.340′	70°57.627′	0.705072	Barberena et al., 2020
19	Combarbalá	W. Principal Cordillera	Rodentia	31°11.372′	70°59.793′	0.704083	Barberena et al., 2020
20	Combarbalá	W. Principal Cordillera	Rodentia	31°11.372′	70°59.793′	0.704131	Barberena et al., 2020
21	Alero Paulino González	W. Principal Cordillera	Rodentia	31°32.756′	70°50.195′	0.704249	Barberena et al., 2020
22	Los Azules 1	W. Principal Cordillera	Rodentia	33°36.906′	70°24.762′	0.70393	Barberena et al., 2017
23	Manzano 1	W. Principal Cordillera	Rodentia	33°33.806′	70°26.568′	0.70396	Barberena et al., 2017
24	Los Queltehues	W. Principal Cordillera	Rodentia	33°54.110′	70°11.333′	0.70401	Barberena et al., 2017
25	Las Cuevas	E. Principal Cordillera	Rodentia	32°48.803′	70°2.148′	0.705557	Barberena et al., 2020
26	Las Cuevas	E. Principal Cordillera	Rodentia	403034.84	70°2.148′	0.705566	Barberena et al., 2020
27	Las Cuevas	E. Principal Cordillera	Rodentia	403034.84	70°2.148′	0.705276	Barberena et al., 2020
28	Laguna del Diamante	E. Principal Cordillera	*Ctenomys* sp.	34°11.835′	69°42.318′	0.707028	Barberena et al., 2020
29	Laguna del Diamante	E. Principal Cordillera	Rodentia	34°11.953′	69°40.579′	0.706000	Barberena et al., 2020
30	Las Cuevas 1	E. Principal Cordillera	*Eligmodontia* sp.	32°48.804′	70°2.150′	0.70567	Barberena et al., 2019
31	Las Cuevas 2	E. Principal Cordillera	*Eligmodontia* sp.	32°48.804′	70°2.150′	0.70567	Barberena et al., 2019
32	Aconcagua 1	E. Principal Cordillera	Rodentia	32°42.301′	69°57.921′	0.70557	Barberena et al., 2019
33	Gendarmería. L. Diamante	Frontal Cordillera	Rodentia	34°11.429′	69°42.685′	0.70655	Barberena et al., 2017
34	Quebrada de La Manga	Frontal Cordillera	Rodentia	32°56.650′	69°18.984′	0.707626	Barberena et al., 2020
35	Quebrada de La Manga	Frontal Cordillera	Rodentia	32°56.650′	69°18.984′	0.707750	Barberena et al., 2020
36	Quebrada de La Manga	Frontal Cordillera	*Ctenomys* sp.	32°56.650′	69°18.984′	0.70799	Barberena et al., 2019
37	Paramillos	Frontal Cordillera	Rodentia	32°28.931′	69°8.099′	0.707288	Barberena et al., 2020
38	Paramillos	Frontal Cordillera	Rodentia	32°28.931′	69°8.099′	0.707579	Barberena et al., 2020
39	Alero Tunduqueral	Precordillera (Uspallata)	Rodentia	32°31.819′	69°18.837′	0.70864	Barberena et al., 2017
40	Alero Tunduqueral	Precordillera (Uspallata)	*Ctenomys* sp.	32°31.819′	69°18.837′	0.70849	Barberena et al., 2019
41	Barrio Ramos	Precordillera (Uspallata)	Rodentia	32°35.480′	69°20.653′	0.709194	Barberena et al., 2020
42	San Ignacio	Precordillera	*Galea* sp.	32°57.367′	69°10.700′	0.70910	Barberena et al., 2019
43	San Ignacio	Precordillera	Rodentia	32°57.367′	69°10.700′	0.708230	Barberena et al., 2020
44	San Ignacio	Precordillera	Rodentia	32°57.367′	69°10.700′	0.710457	Barberena et al., 2020
45	Los Conitos	Precordillera	Rodentia	32°57.697′	69°9.409′	0.710907	Barberena et al., 2020
46	Los Conitos	Precordillera	Rodentia	32°57.697′	69°9.409′	0.709528	Barberena et al., 2020
47	Los Conitos 1	Precordillera	*Galea* sp.	32°57.657′	69°9.403′	0.71026	Barberena et al., 2019
48	Los Conitos 2	Precordillera	*Phyllotis* sp.	32°57.657′	69°9.403′	0.70950	Barberena et al., 2019
49	Agua de la Cueva	Precordillera	*Phyllotis* sp.	32°37.017′	69°9.818′	0.71008	Barberena et al., 2019
50	Agua de la Cueva	Precordillera	*Ctenomys* sp.	32°37.017′	69°9.818′	0.71016	Barberena et al., 2019
51	Agua de la Cueva	Precordillera	Rodentia	32°37.017′	69°9.818′	0.710480	Barberena et al., 2020
52	Agua de la Cueva	Precordillera	Rodentia	32°37.017′	69°9.818′	0.710039	Barberena et al., 2020
53	COINCE. San Carlos	Active foreland	Rodentia	33°40.271′	68°59.139′	0.70732	Barberena et al., 2017

(Continued)

TABLE 3 | Continued

N	Site	Geological unit	Taxon	Latitude (S)	Longitude (W)	$^{87}Sr/^{86}Sr$	Source
54	Barrancas B61	Active foreland	Rodentia	33°5.720′	68°44.820′	0.70666	Barberena et al., 2017
55	Barrancas B61	Active foreland	*Galea* sp.	33°5.720′	68°44.820′	0.70692	Barberena et al., 2019
56	Barrancas B61	Active foreland	*Galea* sp.	33°5.720′	68°44.820′	0.70681	Barberena et al., 2019
57	Natania	Active foreland	*Galea* sp.	32°55.148′	68°51.013′	0.70704	Barberena et al., 2019
58	Divisadero	Active foreland	*Ctenomys* sp.	32°52.640′	68°55.022′	0.70747	Barberena et al., 2019
59	Natania	Active foreland	Rodentia	32°55.148′	68°51.013′	0.706979	Barberena et al., 2020
60	Natania	Active foreland	Rodentia	32°55.148′	68°51.013′	0.706986	Barberena et al., 2020
61	Lavalle	Active foreland	Rodentia	32°23.782′	67°51.077′	0.707564	Barberena et al., 2020
62	Lavalle	Active foreland	Rodentia	32°23.782′	67°51.077′	0.707494	Barberena et al., 2020
63	Capiz Alto	Active foreland	Rodentia	33°40.134′	68°58.702′	0.707015	Barberena et al., 2020
64	Capiz Alto	Active foreland	Rodentia	33°40.134′	68°58.702′	0.707507	Barberena et al., 2020
65	Barrancas B6	Active foreland	Rodentia	33°5.595′	68°44.785′	0.706543	Barberena et al., 2020

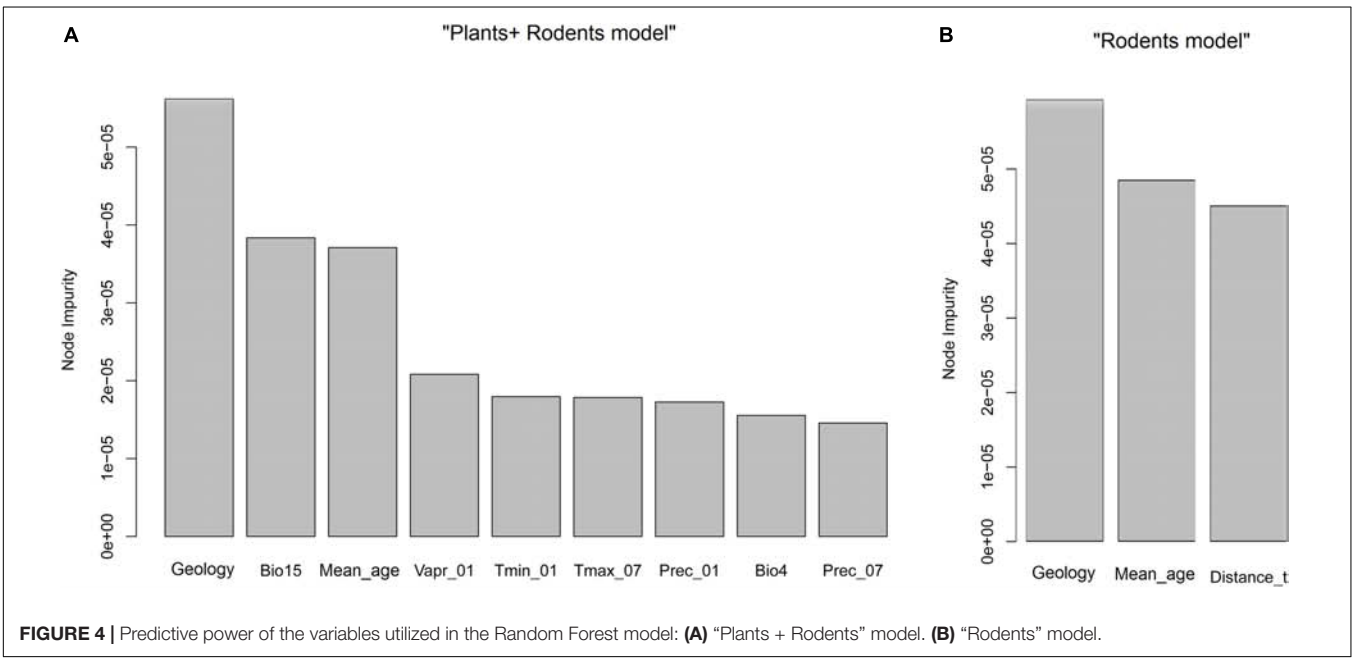

FIGURE 4 | Predictive power of the variables utilized in the Random Forest model: **(A)** "Plants + Rodents" model. **(B)** "Rodents" model.

(Geological Province and Mean-age), while the third (Distance to coast) would be related with the decreasing incidence of marine strontium—0.709202 ± 0.000003—(Kuznetsov et al., 2012) with increasing distance from the coast (Alonzi et al., 2020). Importantly, in the "Plants + Rodents" model several bioclimatic variables contribute to structure variation with a substantial role of temperature seasonality (Bio15).

The analysis of the linear fit between the predicted and observed $^{87}Sr/^{86}Sr$ values shows that the plant samples have a larger estimation error than the rodent samples, likely affecting the amount of variation, respectively, explained by the two Random Forest models presented, as well as the number of variables selected by each model (9 in the "Plants + Rodents" model vs. 3 in the "Rodents" model, **Figure 4**). In the "Plants + Rodents" model the validation of the Random Forest model with the new cases from the test set (20% of the sample) accounts for 72% of the variation (R-squared = 0.72) with a RMSE = 0.0008. The Mantel test produces a value of $r = -0.07$, $p > 0.05$, suggesting that there is no significant remaining spatial structure in the residuals, although a low autocorrelation was detected in two distance intervals (**Supplementary Figure 1A**). While the linear regression between the values included in the training and testing sets for the "Plants + Rodents" samples shows a good overall fit, there is a larger dispersion of the residuals in the area of the most radiogenic values—between 0.709 and 0.710—(**Figures 5A,B**). In the SAST, these samples are located adjacent or within the Precordillera highlands (including the Uspallata Valley), formed by Lower Paleozoic rocks that are the oldest present (**Figure 2**). This increase in the magnitude of residual values in contexts with higher $^{87}Sr/^{86}Sr$ ratios has been shown to be a global phenomenon (Bataille et al., 2020) and explains the existence of considerably higher residuals in the "Plants + Rodents" model compared to the "Rodents" model (**Figures 5B,D**).

The regression between the predicted and observed results for the "Rodents" sample shows a high fit between predicted

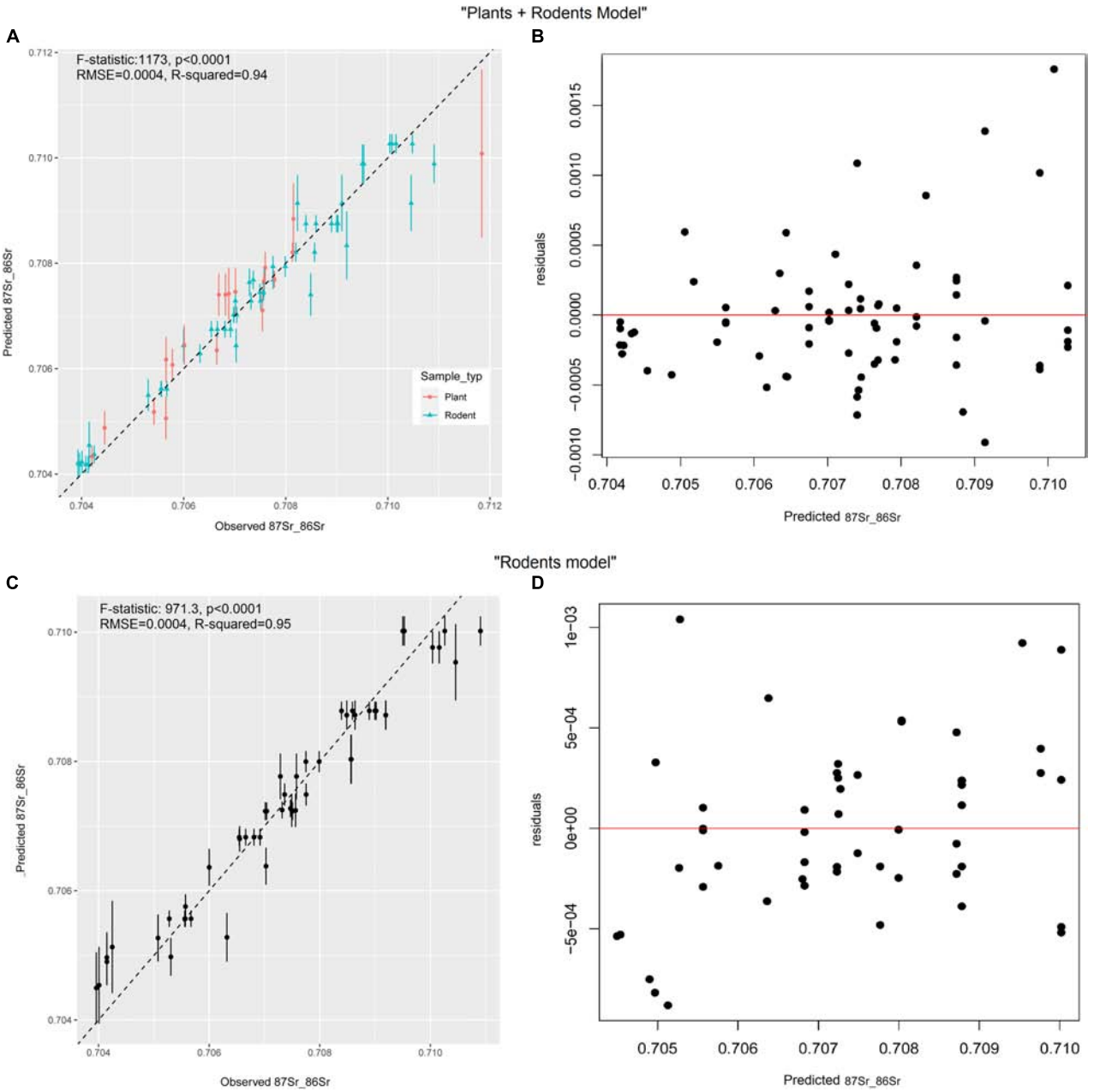

FIGURE 5 | Linear regression between predicted and observed $^{87}Sr/^{86}Sr$ values and associated residuals: **(A,B)** "Plants + Rodents" model. **(C,D)** "Rodents" model.

and observed $^{87}Sr/^{86}Sr$ values (**Figure 5C**) and the validation of the Random Forest model with the new cases from the test set (20% of the sample) accounts for 95% of the variation (*R*-squared = 0.95, RMSE = 0.003) (**Figures 5C,D**). The Mantel test produces a value of $r = 0.005$, $p > 0.05$, suggesting that there is no remaining spatial structure in the residuals (**Supplementary Figure 1B**). In **Supplementary Figure 1** we present the isoscapes with the Standard Error, Quartile 1 (25%), Quartile 3 (median), and Quartile 3 (75%). In the **Supplementary Materials** file we also present the results for all the covariates analyzed in this model.

The analysis of partial dependence between the predictor variables and $^{87}Sr/^{86}Sr$ values for the "Plants + Rodents" model suggests an eastwards exponential increase of the values beyond 150 km from the Pacific coast, reaching the highest values at a distance of 250 km from the coast (**Figure 6**). This is compatible with the underlying trends in bedrock age from west to east, characterized by the succession of increasingly older rocks: Western Principal Cordillera (Oligocene-Pliocene), Eastern Principal Cordillera (Cretaceous-Jurassic), Frontal Cordillera (Permian-Triassic), and Precordillera (Lower Paleozoic) (**Figure 2**). Eastwards from

Precordillera, there is a decrease in $^{87}Sr/^{86}Sr$ values in the Active Foreland, a Quaternary basin that averages sediments from Precordillera and younger formations such as the Cordillera Frontal and Cordillera Principal (**Figure 6A**). While sampling is small in these Quaternary deposits, it is expected that spatial resolution will be lower compared to the Andes (see below).

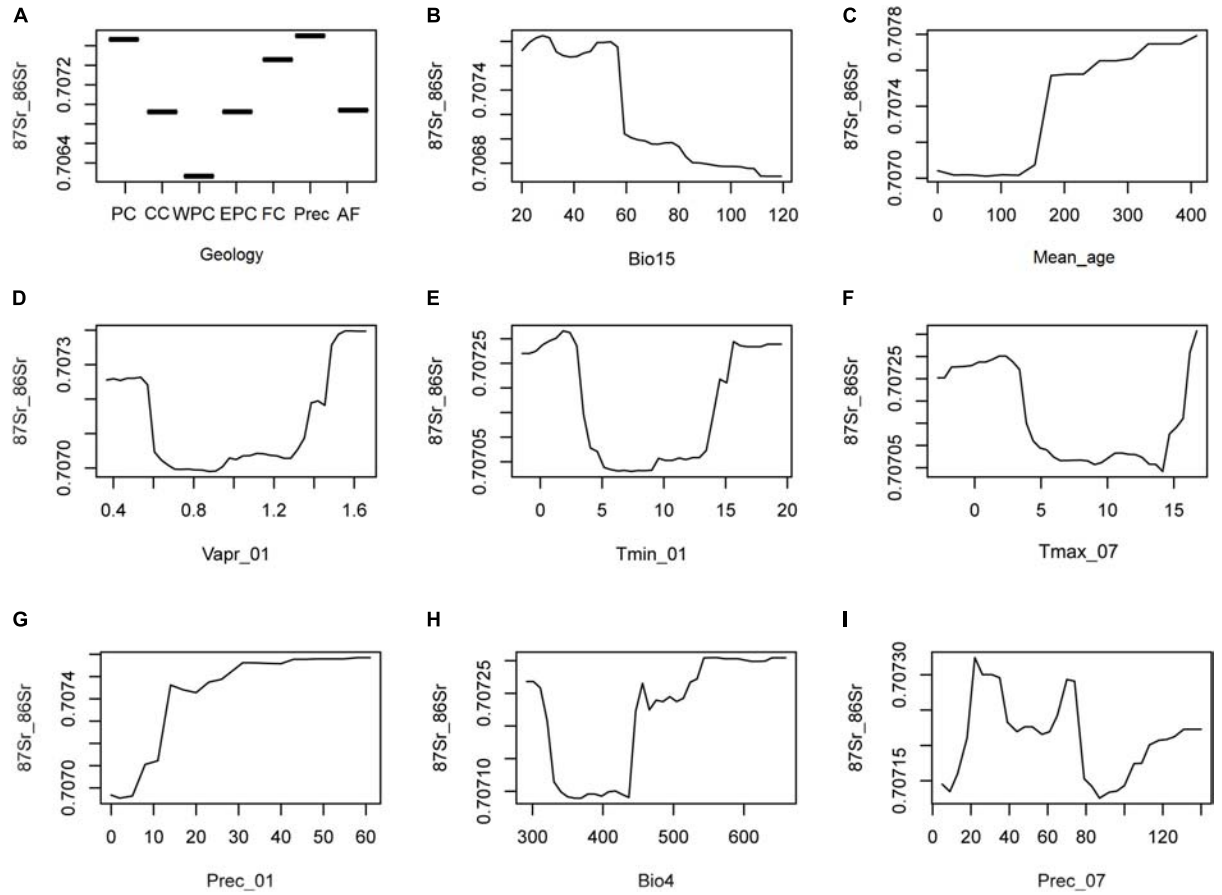

FIGURE 6 | Analysis of partial dependence between the variables of the Random Forest models and $^{87}Sr/^{86}Sr$ values for the "Plants + Rodents" model. Key: **(A)** geological province, **(B)** temperature seasonality, **(C)** mean rock age (years), **(D)** evapotranspiration January, **(E)** minimum temperature January, **(F)** maximum temperature July, **(G)** precipitations January, **(H)** precipitation seasonality, and **(I)** precipitation July.

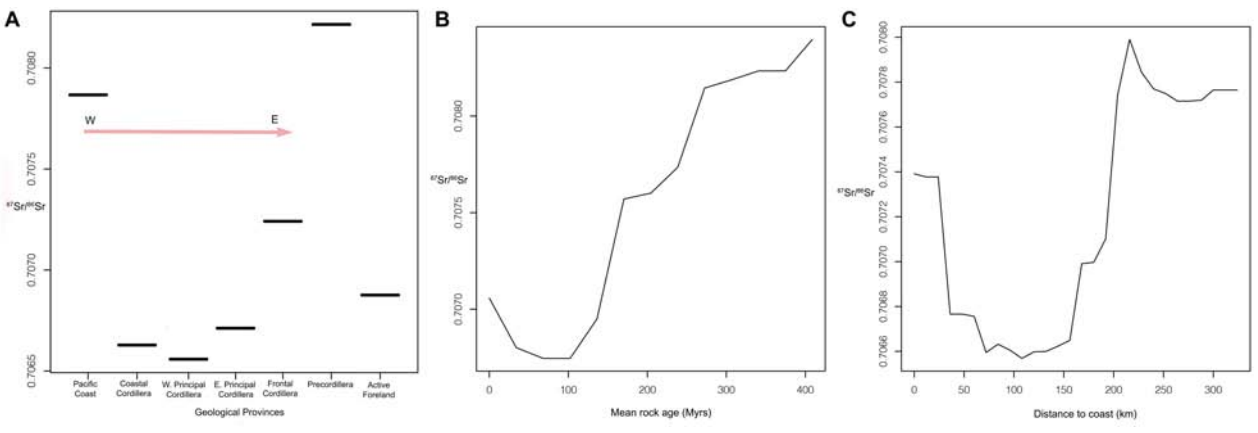

FIGURE 7 | Analysis of partial dependence between the variables of the Random Forest models and $^{87}Sr/^{86}Sr$ values for the "Rodents" model. Key: **(A)** geological province, **(B)** mean rock age (years), and **(C)** distance to coast (km).

The most important bioclimatic variable identified is *Bio15*, a coefficient of Seasonality based on temperature, followed by *Tmin07*—Minimum July temperature.

The "Rodents" model, on the other hand, is accounted for in a much more simplified fashion by only three predictor variables: Geology, Mean-age, and Distance to coast (**Figure 7**), indicating that the rodent samples track the geological variation more closely than the "Plants + Rodents" model, where several bioclimatic variables contribute significantly.

Isoscape for the Southern Andean Strontium Transect

We have presented the results for bioavailable strontium across the SAST connecting the Pacific Ocean in Chile and the eastern lowlands in Argentina. The application of the Random Forest approach pioneered by Bataille et al. (2018) has allowed comparing two substrates that can be used to build frames of reference for the interpretation of $^{87}Sr/^{86}Sr$ values in archeological remains. The "Rodents" model presents the best fit between predicted and observed values (85%) in association with a small error (RMSE = 0.0007). This large amount of variation can be accounted for with a simpler model where only the predictors Geological province, Mean rock age, and Distance to coast explain the observed variation, whereas in the "Plants + Rodents" model several bioclimatic variables—particularly seasonality of precipitation (Bio15)—contribute to explain variation in addition to geological province and Mean-age (**Figures 6**, **7**). Considering that the plant samples analyzed are modern, an issue that will need to be explored in the future is the possible incidence of modern mining activities in the $^{87}Sr/^{86}Sr$ values in plants (Burger and Lichtscheidl, 2019; Thomsen and Andreasen, 2019).

While this project was not formally designed to compare alternative substrates to build strontium isoscapes, we suggest that by its higher fidelity to bedrock geology, rock age, and distance to coast, rodents provide a more accurate proxy for the interpretation of values in human remains in our study area (Price et al., 2002; Bentley, 2006). In **Figure 8A** we present the strontium isoscape and the associated residual values (**Figure 8B**) to assess the uncertainty of the isoscape across the SAST.

SCALE OF HUMAN MOBILITY AND MIGRATION IN THE SOUTHERN ANDES: A REGIONAL CASE-STUDY

We have recently reported $^{87}Sr/^{86}Sr$ values for 38 human samples (12 teeth and 26 bones) from 30 individuals from seven archeological sites in the Andean Uspallata Valley in Northwestern Mendoza province, Argentina, which span the period between AD 800–1500 and encompass the conquest by the Inka Empire starting ca. AD 1410 (Barberena et al., 2020; **Table 4**). The economic basis during this period would have been highly variable across space and time with multiple combinations of wild plants, the wild camelid guanaco—*Lama guanicoe*—, the domestic llama—*Lama glama*—, and several cultivated plants including maize, squash, chinoa, and beans (Frigolé and Gasco, 2016; Ots et al., 2016; Gil et al., 2020). In this context, the spatial scale of human territories was likely variable through time and remains as an issue of considerable debate. In order to tackle this issue directly, we next apply the newly presented strontium isoscape derived from the Random Forest approach to reconstruct the geographic range of the individuals analyzed from the inter-mountain Uspallata Valley (see location **Figure 1** and landscape in **Figure 3e**).

The results have a bimodal distribution with two non-overlapping groups determined by mixture analysis: the first one is composed of 27 samples with a mean of 0.7090 ± 0.0003 (range: 0.7083–0.7095) and the second group is composed of 11 samples with a mean of 0.7073 ± 0.0001 (range: 0.7072–0.7075). These groups are significantly different statistically (Mann-Whitney $z = 4.7637$, $p = 0.0001$). The geographic allocation produced with the random forest strontium isoscape indicates that the first

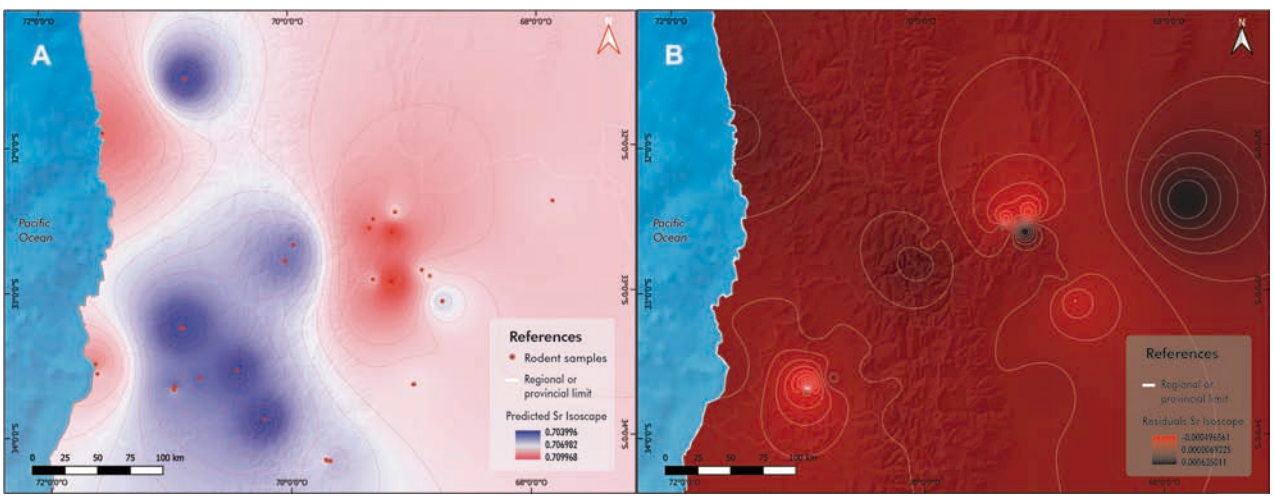

FIGURE 8 | "Rodents" model: **(A)** Random Forest bioavailable strontium isoscape. **(B)** Associated uncertainty.

TABLE 4 | $^{87}Sr/^{86}Sr$ results and contextual information for human remains from the Uspallata Valley, northwestern Mendoza, Argentina (from Barberena et al., 2020).

Site	Individual	Latitude (S)	Longitude (W)	^{14}C age (BP)	Calibrated range (AD)	Sex	Age (years)	Tissue	$^{87}Sr/^{86}Sr$
Barrio Ramos I	1	32°35.480′	69°20.653′	583 ± 43	1310–1450	M?	35–40	rib	0.709582
Barrio Ramos I	1	32°35.480′	69°20.653′	583 ± 43	1310–1450	M?	35–40	I	0.709333
Barrio Ramos I	2	32°35.480′	69°20.653′	583 ± 43	1310–1450	M	40–50	LC	0.70901
Barrio Ramos I	2	32°35.480′	69°20.653′	583 ± 43	1310–1450	M	40–50	rib	0.70953
Barrio Ramos I	3	32°35.480′	69°20.653′	583 ± 43	1310–1450	F	>40	I2	0.70865
Barrio Ramos I	3	32°35.480′	69°20.653′	583 ± 43	1310–1450	F	>40	rib	0.70922
Monte de Algarrobos	1219	32°36.345′	69°20.932′	298 ± 28	1500–1800	F	Adult	rib	0.70757
Monte de Algarrobos	1219	32°36.345′	69°20.932′	298 ± 28	1500–1800	F	Adult	I^2 right	0.709128
Usina Sur 2	1	32°38.055′	69°22.467′	772 ± 25	1220–1380	ND	Adult	rib	0.707462
Usina Sur 2	2	32°38.055′	69°22.467′	772 ± 25	1220–1380	ND	Adult	Molar	0.707504
Túmulo I	n/n 1	32°35.23′	69°21.61′	977 ± 35	1020–1190	ND	Adult	1st metatarsal	0.709443
Túmulo I	n/n 2	32°35.23′	69°21.61′	977 ± 35	1020–1190	ND	Young adult	1st metatarsal	0.709378
Túmulo I	n/n 3	32°35.23′	69°21.61′	977 ± 35	1020–1190	ND	Adult	1st metatarsal	0.709528
Túmulo I	n/n 4	32°35.23′	69°21.61′	977 ± 35	1020–1190	ND	Adult	1st metatarsal	0.709156
Túmulo II	237	32°35.23′	69°21.61′			N/D	2.5–4	rib	0.708931
Túmulo II	238	32°35.23′	69°21.61′			F?	8–9	I dentine-enamel	0.709073
Túmulo II	239	32°35.23′	69°21.61′	1269 ± 35	680–890	F	>50	rib	0.709188
Túmulo II	239	32°35.23′	69°21.61′	1269 ± 35	680–890	F	>50	I_2/M2	0.708635
Túmulo II	240	32°35.23′	69°21.61′			M	40–49	rib	0.709019
Túmulo II	240	32°35.23′	69°21.61′			M	40–49	I_2 right	0.708342
Túmulo II	241	32°35.23′	69°21.61′			ND	35–45	rib	0.709164
Túmulo II	242	32°35.23′	69°21.61′			M	18–23	rib	0.709002
Túmulo II	242	32°35.23′	69°21.61′			M	18–23	I^2 right dentine-enamel	0.708639
Túmulo II	243	32°35.23′	69°21.61′	1178 ± 41	770–1020	F	40–49	calcaneous	0.709098
Túmulo II	243	32°35.23′	69°21.61′	1178 ± 41	770–1020	F	40–49	I dentine/M3	0.708497
Túmulo II	244	32°°35.23′	69°21.61′			F	39–45	molar	0.709026
Túmulo II	245	32°35.23′	69°21.61′			M	35–45	rib	0.709038
Túmulo II	245	32°35.23′	69°21.61′			M	35–45	I_2 right	0.709035
Túmulo III	n/n 1	32°35.23′′	69°21.61′	671 ± 40	1290–1400	ND	Adult	1st metatarsal	0.708955
Túmulo III	n/n 2	32°35.23′	69°21.61′	671 ± 40	1290–1400	ND	Adult	1st metatarsal	0.70879
Túmulo III	n/n 3	32°35.23′	69°21.61′	671 ± 40	1290–1400	ND	Adult	1st metatarsal	0.707267
Potrero Las Colonias	n/n 1	32°36.555′	69°21.724′	568 ± 38	1320–1450	ND	Sub-adult	1st metatarsal	0.707251
Potrero Las Colonias	n/n 2	32°36.555′	69°21.724′	634 ± 28	1300–1420	ND	Adult	1st metatarsal	0.70732
Potrero Las Colonias	n/n 3	32°36.555′	69°21.724′	682 ± 25	1290–1400	ND	Adult	1st metatarsal	0.707343
Potrero Las Colonias	n/n 4	32°36.555′	69°21.724′	682 ± 25	1290–1400	ND	Adult	1st metatarsal	0.707252
Potrero Las Colonias	n/n 5	32°36.555′	69°21.724′	682 ± 25	1290–1400	ND	Adult	1st metatarsal	0.707407
Potrero Las Colonias	n/n 6	32°36.555′	69°21.724′	682 ± 25	1290–1400	ND	Adult	1st metatarsal	0.707243
Potrero Las Colonias	n/n 7	32°36.555′	69°21.724′	682 ± 25	1290–1400	ND	Adult	1st metatarsal	0.707401

group of individuals—from the sites Túmulo I, Túmulo II, and Barrio Ramos I—had a relatively restricted range of paleomobility which includes the Uspallata Valley and immediately adjacent areas of Precordillera and Cordillera Frontal (**Figure 9**). While the isoscape also points to the Pacific coast as a possible area of residence, this alternative can be ruled out on the basis of paleodietary information that does not suggest any intake of marine foods (Gil et al., 2014; Barberena et al., 2020). In addition, the organization of lithic and ceramic technology offer evidence compatible with restricted human territories for the period between AD 500 and 1000 in the inter-mountain Potrerillos Valley, adjacent to the Precordillera and close to Uspallata (Cortegoso, 2006; Frigolé and Gasco, 2016). While it certainly cannot be inferred that these groups were sedentary, we suggest that this first group of analyzed individuals had a local scale of mobility centered around Uspallata and not systematically connecting with the eastern lowlands nor the western Andean shed. Building on this, and also supported by the presence of multiple cemeteries, it can be suggested that Uspallata witnessed a sustained occupation by groups tethered to the valley (Barberena et al., 2017, 2020).

Regarding the second group of individuals—from the sites Potrero Las Colonias, Usina Sur 2, and Túmulo III—, the isoscape suggests that they had a disjunct geographic range and did not reside in Uspallata for a significant amount of time. While the precise geographic area of origin of these individuals cannot be precisely determined yet, the geographic analysis identifies some possible—if not the only—sources. Hence, we

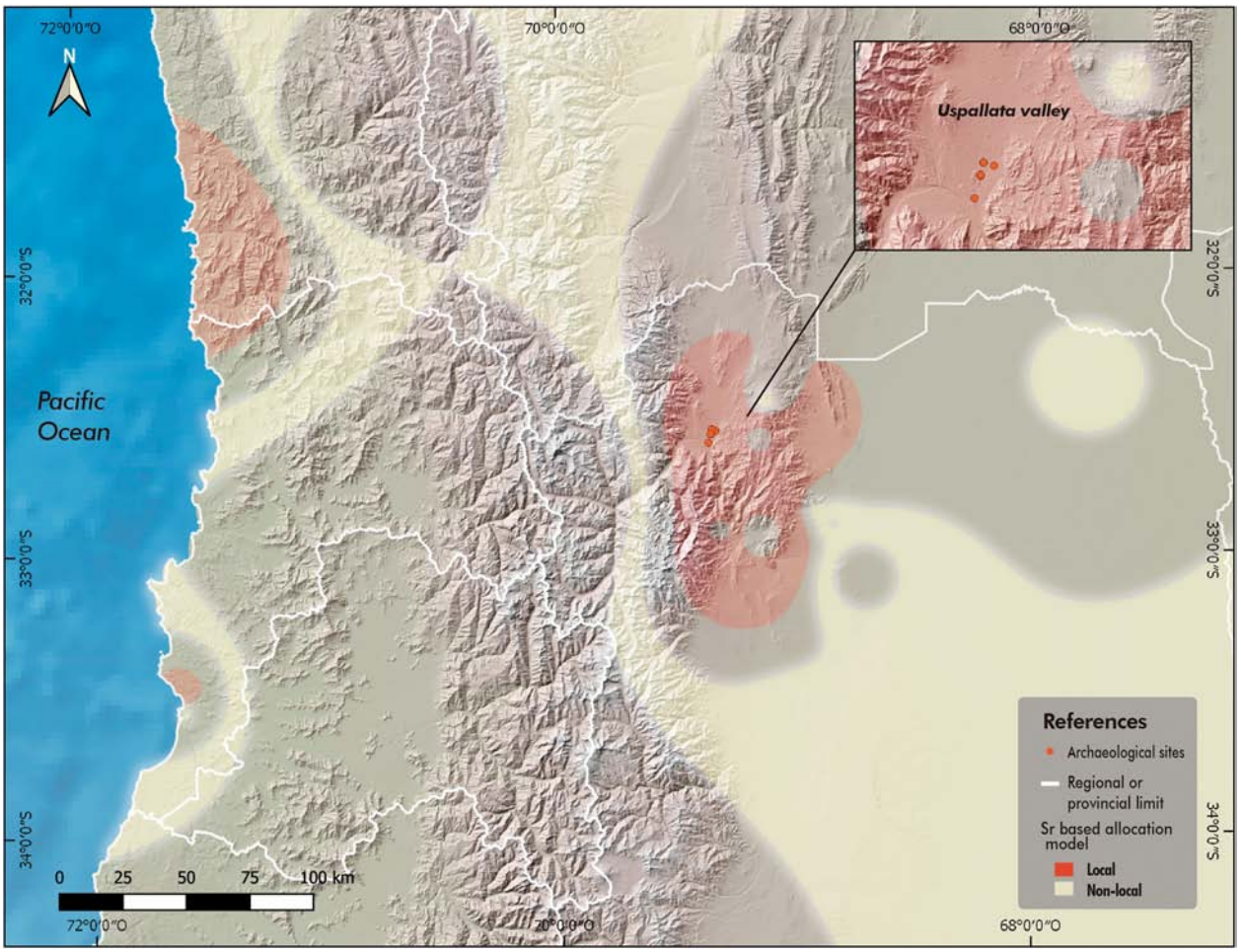

FIGURE 9 | Geographical allocation of local and non-local individuals from the Uspallata Valley (Mendoza Province, Argentina).

argue that these individuals, tough buried in Uspallata, can be interpreted as migrants.

Interestingly, there is a patterned temporal trend in the distribution of these two isotopic groups. The 27 local samples come from four sites spanning AD 800–1500, which indicates the continuous presence of locals in the Valley until the Inka arrival ∼AD 1410 (Marsh et al., 2017). On the other hand, the non-local individuals are temporally clustered between AD 1280 and 1420, a brief phase that includes 10 of the 11 non-local individuals. This immigration pulse shortly precedes the initial presence of the Inka in Uspallata, leading us to suggest that there was a multicultural social setting when the Empire arrived. This entails a more complex dynamic of interaction between the Inka and the diverse preexisting local societies in the southern periphery (Garrido, 2016; Durán V. A. et al., 2018; Troncoso, 2018; Pavlovic et al., 2019).

CONCLUSION AND PERSPECTIVES

The bioavailable strontium isoscape reconstructed for the SAST by means of Random Forest can be compared with recent macro-regional results presented for northern Patagonia (Serna et al., 2020), southwards from our study area. Serna et al. (2020) record limited strontium isotopic variation which is not strongly related to bedrock geology. Specifically, they identify a gradual increase in $^{87}Sr/^{86}Sr$ eastwards inversely correlated with elevation and positively correlated with the rate of dust deposition, which are selected by the model as the main variables accounting for the observed variation. Building on these finds, the authors suggest that the deposition and reworking of unradiogenic volcanic sediments by aeolian, fluvial, and glacial erosion homogenized the isotopic landscape, decoupling to some extent bioavailable variation from underlying bedrock geology. This study indicates that recent geomorphic processes have an impact in the spatial resolution in terms of that can be achieved by means of bioavailable $^{87}Sr/^{86}Sr$ data to assess past landscape use (Crowley and Godfrey, 2019; Scaffidi and Knudson, 2020; Scaffidi et al., 2020; Serna et al., 2020; Snoeck et al., 2020; Miller et al., 2021).

Our results for the southern Andes of Argentina and Chile show a different picture, particularly regarding rodent values, where there is large isotopic variation and a very tight correlation with bedrock geology, mean rock age, and

distance to coast, which altogether allow building a robust model accounting for 85% of the observed variation with little associated uncertainty across space—as measured by the residuals between predicted and observed values. Our results suggest that bioavailable strontium is tightly linked with bedrock geology and offers a highly resolved proxy to track human paleogeography involving the complementary levels of territories or daily mobility anomalous events that disrupt home ranges, such as migration (Barberena et al., 2020). By combining these different studies guided by the Random Forest approach we can learn about the geological and biophysical variables that contribute to structure the observed isotopic variation, thus calibrating the spatial resolution that can be achieved for each study area. The global bedrock model of expected strontium values (Bataille et al., 2020) is not selected as a strong predictor variable in these two studies. As Bataille et al. (2020) suggest, this model has a larger associated error for regions that are data-poor, have geologies that fall outside of the calibration dataset originally employed, or have outdated geology maps in the GLiM database utilized by the model. South America is one of the world regions that can be considered as still under-studied in this regard (Bataille et al., 2020).

At a regional scale of archeological analysis, the application of the southern Andean isoscape to geographically allocate archeological human remains from the Uspallata Valley shows promising results at two complementary levels: first, it confirms the persistence of human groups with relatively restricted territories encompassing Uspallata-Precordillera between the period AD 800 and 1,500. This reduced mobility is well-grounded in the isoscape-based analysis and goes against previous interpretations of high residential mobility across altitudinal regions developed on the basis of $\delta^{18}O$ values (Ugan et al., 2012). Secondly, we have identified a pulse of migration from a still undetermined region that shortly precedes the Inka conquest of the southern frontier of the Empire. Stable carbon isotopes results suggest that these migrants were intensive maize-farmers (Barberena et al., 2020). In synthesis, we have been able to analyze the daily (territories) and anomalous (migration) spheres of mobility making up human paleogeography in the southern Andes in all its complexity. Based on this first large-scale approach to bioavailable strontium across the southern Andes of Argentina and Chile, it will be possible to move forward in comparing the spatial resolution offered by different isotopic proxies of human paleomobility in diverse geographic and climatic contexts (Ugan et al., 2012; Knudson et al., 2014b; Barberena et al., 2017; Grimstead et al., 2017; Bataille et al., 2018; Willmes et al., 2018; Serna et al., 2019; Snoeck et al., 2020). Finally, we expect that the project presented here will converge with other ongoing efforts in the South-Central Andes (Scaffidi and Knudson, 2020) and northern Patagonia (Serna et al., 2020) to build a pan-Andean frame of research to track the movement of people, animals and artifacts across space and time in South America.

DATA AVAILABILITY STATEMENT

The isotopic, Random Forest results, and the R code produced in this study are fully included in the article/**Supplementary Material**. Further inquiries can be directed to the corresponding authors.

AUTHOR CONTRIBUTIONS

RB designed research. RB, CL, AG, AN-D, EM, CF, LC, FF, LS, AT, FS, VC, VD, and CM collected samples for analysis. RB, AT, CL, and AG prepared the samples for lab analyses. PL was in charge of isotopic analyses. MC conducted the Machine Learning analysis. GL developed the GIS construction of isoscapes. DW and AB built the geological framework. RB, MC, GL, and CM wrote the manuscript with contributions from all authors.

FUNDING

This research was funded by the National Geographic Society (Project HJ-136R-17), Programa Regional ANID 20F0002 (Chile), and PIP-CONICET 0301 (Argentina).

ACKNOWLEDGMENTS

We acknowledge Consejo Nacional de Investigaciones Científicas y Técnicas (CONICET), the Insrtituto Interdisciplinario de Ciencias Básicas (ICB), and the Universidad Nacional de Cuyo for their continuous support, and the Comisión Nacional de Energía Atómica (San Rafael) for the help with sample preparation. Clement P. Bataille kindly offered his advice regarding the Random Forest models. Finally, we acknowledge the insightful comments provided by the two reviewers and the guest editors of the volume.

SUPPLEMENTARY MATERIAL

The Supplementary Material for this article can be found online at: https://www.frontiersin.org/articles/10.3389/fevo.2021.584325/full#supplementary-material

REFERENCES

Abraham, E., del Valle, H. F., Roig, F., Torres, L., Ares, J. O., Coronato, F., et al. (2009). Overview of the geography of the monte desert biome (Argentina). *J. Arid Environ.* 73, 144–153. doi: 10.1016/j.jaridenv.2008.09.028

Alonzi, E., Pacheco-Forés, S. I., Gordon, G. W., Kuijt, I., and Knudson, K. J. (2020). New understandings of the sea spray effect and its impact on bioavailable radiogenic strontium isotope ratios in coastal environments. *J. Archaeol. Sci. Rep.* 33:102462. doi: 10.1016/j.jasrep.2020.102462

Andrushko, V. A., Buzon, M. R., Gibaja, A. M., McEwan, G. F., Simonetti, A., and Creaser, R. A. (2011). Investigating a child sacrifice event from the Inca heartland. *J. Archaeol. Sci.* 38, 323–333. doi: 10.1016/j.jas.2010.09.009

Astini, R. A., Benedetto, J. L., and Vaccari, N. E. (1995). The early paleozoic evolution of the argentine precordillera as a laurentian rifted, drifted, and collided terrane: a geodynamic model. *Geol. Soc. Am. Bull.* 107, 253–273. doi: 10.1130/0016-7606(1995)107<0253:tepeot>2.3.co;2

Banner, J. L. (2004). Radiogenic isotopes: systematics and applications to earth surface processes and chemical stratigraphy. *Earth Sci. Rev.* 65, 141–194. doi: 10.1016/s0012-8252(03)00086-2

Barberena, R., Durán, V. A., Novellino, P., Winocur, D., Benítez, A., Tessone, A., et al. (2017). Scale of human mobility in the southern Andes (Argentina and Chile): a new framework based on strontium isotopes. *Am. J. Phys. Anthropol.* 164, 305–320. doi: 10.1002/ajpa.23270

Barberena, R., Menéndez, L., Novellino, P., Lucero, G., Luyt, J., Sealy, J., et al. (2020). Multi-isotopic and morphometric evidence for the migration of farmers leading up to the Inka conquest of the southern Andes. *Sci. Rep.* 10:21171.

Barberena, R., Tessone, A., Cagnoni, M., Gasco, A., Durán, V., Winocur, D., et al. (2019). Bioavailable strontium in the southern andes (argentina and chile): a tool for tracking human and animal movement. *Environ. Archaeol. in press*. doi: 10.1080/14614103.2019.1689894

Bárcena, J. R. (2001). "Prehistoria del centro-oeste argentino," in *Historia Argentina Prehispánica*, eds E. Berberian and A. E. Nielsen (Córdoba: Brujas), 561–634.

Bataille, C. P., Brennan, S. R., Hartmann, J., Moosdorf, N., Wooller, M. J., and Bowen, G. J. (2014). A geostatistical framework for predicting variations in strontium concentrations and isotope ratios in Alaskan rivers. *Chem. Geol.* 389, 1–15. doi: 10.1016/j.chemgeo.2014.08.030

Bataille, C. P., Crowley, B. E., Wooller, M. J., and Bowen, G. J. (2020). Advances in global bioavailable strontium isoscapes. *Palaeogeogr. Palaeoclimatol. Palaeoecol.* 555:109849. doi: 10.1016/j.palaeo.2020.109849

Bataille, C. P., von Holstein, I. C. C., Laffoon, J. E., Willmes, M., Liu, X.-M., and Davies, G. R. (2018). A bioavailable strontium isoscape for Western Europe: a machine learning approach. *PLoS One* 13:e0197386. doi: 10.1371/journal.pone.0197386

Bentley, R. A. (2006). Strontium Isotopes from the Earth to the Archaeological skeleton: a review. *J. Archaeol. Method Theory* 13, 135–187. doi: 10.1007/s10816-006-9009-x

Bjornstad, O. N., and Cai, J. (2020). *ncf: Spatial Covariance Functions*. Available online at: https://CRAN.R-project.org/package=ncf [accessed July 14, 2020].

Borić, D., and Price, T. D. (2013). Strontium isotopes document greater human mobility at the start of the Balkan Neolithic. *Proc. Natl. Acad. Sci. U.S.A.* 110, 3298–3303. doi: 10.1073/pnas.1211474110

Breiman, L. (2001). Random forests. *Mach. Learn.* 45, 5–32.

Burger, A., and Lichtscheidl, I. (2019). Strontium in the environment: review about reactions of plants towards stable and radioactive strontium isotopes. *Sci. Total Environ.* 653, 1458–1512. doi: 10.1016/j.scitotenv.2018.10.312

Capo, R. C., Stewart, B. W., and Chadwick, O. A. (1998). Strontium isotopes as tracers of ecosystem processes: theory and methods. *Geoderma* 82, 197–225. doi: 10.1016/s0016-7061(97)00102-x

Chala-Aldana, D., Bocherens, H., Miller, C., Moore, K., Hodgins, G., and Rademaker, K. (2018). Investigating mobility and highland occupation strategies during the early holocene at the cuncaicha rock shelter through strontium and oxygen isotopes. *J. Archaeol. Sci. Rep.* 19, 811–827. doi: 10.1016/j.jasrep.2017.10.023

Charrier, R., Baeza, O., Elgueta, S., Flynn, J. J., Gans, P., Kay, S. M., et al. (2002). Evidence for cenozoic extensional basin development and tectonic inversion south of the flat-slab segment, southern central andes. Chile (33°–36°S.L.). *J. S. Am. Earth Sci.* 15, 117–139. doi: 10.1016/s0895-9811(02)00009-3

Clapperton, C. (1993). *Quaternary Geology and Geomorphology of South America*. Amsterdam: Elsevier.

Copeland, S. R., Cawthra, H. C., Fisher, E. C., Lee-Thorp, J. A., Cowling, R. M., le Roux, P. J., et al. (2016). Strontium isotope investigation of ungulate movement patterns on the pleistocene paleo-agulhas plain of the greater cape floristic region, South Africa. *Quat. Sci. Rev.* 141, 65–84. doi: 10.1016/j.quascirev.2016.04.002

Copeland, S. R., Sponheimer, M., Lee-Thorp, J. A., De Ruiter, D. J., Le Roux, P. J., Grimes, V., et al. (2010). Using strontium isotopes to study site accumulation processes. *J. Taphonomy* 8, 115–127.

Cornejo, L. (2014). Sobre la cronología de la imposición cuzqueña en Chile. *Estudios Atacameños* 47, 101–116.

Cornejo, L. E., Jackson, D., and Saavedra, M. (2016). "Cazadores-rccolectores arcaicos al sur del desierto (ca. 11.000 a 300 años a.C.)," in *Prehistoria en Chile. Desde sus Primeros Habitantes Hasta Los Incas*, eds F. Falabella, M. Uribe, L. Sanhueza, C. Aldunate, and J. Hidalgo (Santiago de Chile: Sociedad Chilena de Arqueología), 285–317.

Cornejo, L., and Sanhueza, L. (2011). Caminos que cruzan la cordillera: el rol del paso del maipo en la ocupación de la cordillera en chile central. *Revista Chilena de Antropología*. 23, 101–122.

Cortegoso, V. (2006). Comunidades agrícolas en el Valle de Potrerillos (NO de Mendoza) durante el Holoceno tardío: organización de la tecnología y vivienda. *Intersecciones en Antropología* 7, 77–94

Cortegoso, V., Barberena, R., Durán, V., and Lucero, G. (2016). Geographic vectors of human mobility in the Andes (34–36° S): comparative analysis of 'minor' obsidian sources. *Quat. Int.* 422, 81–92. doi: 10.1016/j.quaint.2015.11.133

Crowley, B. E., and Godfrey, L. R. (2019). Strontium isotopes support small home ranges for extinct lemurs. *Front. Ecol. Evol.* 7:490.

Dantas, M., and Knudson, K. J. (2016). Isótopos de estroncio: cría, circulación y apropiación de camélidos en Aguada de Ambato (Catamarca. Argentina). *Intersecciones en Antropología* 17, 239–250.

Díaz, S., Cabido, M., Zak, M., Carretero, E. M., and Araníbar, J. (1999). Plant functional traits, ecosystem structure and land-use history along a climatic gradient in central-western Argentina. *J. Veg. Sci.* 10, 651–660. doi: 10.2307/3237080

Durán, V. A., Cortegoso, V., Barberena, R., Frigolé, C., Novellino, P., Lucero, G., et al. (2018). 'To and fro' the southern Andean highlands (Argentina and Chile): archaeometric insights on geographic vectors of mobility. *J. Archaeol. Sci. Rep.* 18, 668–678. doi: 10.1016/j.jasrep.2017.05.047

Durán, V., Novellino, P., Menéndez, L., Gasco, A., Marsh, E., and Barberena, R. (2018). Barrio ramos i. funebria y modos de vida en el inicio del período de dominación inca del valle de Uspallata (Mendoza, Argentina). *Relaciones de la Sociedad Argentina de Antropología* XLIII(1), 55–86. doi: 10.31819/9783954871704-004

English, N. B., Betancourt, J. L., Dean, J. S., and Quade, J. (2001). Strontium isotopes reveal distant sources of architectural timber in Chaco Canyon, New Mexico. *Proc. Natl. Acad. Sci. U.S.A.* 98, 11891–11896. doi: 10.1073/pnas.211305498

Ericson, J. E. (1985). Strontium isotope characterization in the study of prehistoric human ecology. *J. Hum. Evol.* 14, 503–514. doi: 10.1016/s0047-2484(85)80029-4

Falabella, F., Pavlovic, D., Planella, M. T., and Sanhueza, L. (2016). "Diversidad y heterogeneidad cultural y social en Chile Central durante los períodos Alfarero temprano e Intermedio Tardío (300 años a.C. a 1450 años d.C.)," in *Prehistoria en Chile*, eds F. Falabella, M. Uribe, L. Sanhueza, C. Aldunate, and J. Hidalgo (Santiago de Chile: Sociedad Chilena de Antropología), 365–400.

Fick, S. E., and Hijmans, R. J. (2017). WorldClim 2: new 1-km spatial resolution climate surfaces for global land areas. *Int. J. Climatol.* 37, 4302–4315. doi: 10.1002/joc.5086

Frigolé, C., and Gasco, A. (2016). Potters and herders at the southern edge of the Andean world: risk management and mobility in Northwestern Mendoza. Argentina. *Quat. Int.* 422, 152–162. doi: 10.1016/j.quaint.2016.02.032

Furque, G., and Cuerda, A. J. (1979). Precordillera de la rioja, san juan y mendoza. *Geol. Regional Argentina* 1, 455–522.

García, A. (2003). La ocupación temprana de los Andes centrales argentinos (ca. 11.000-8.000 años C14 AP). *Relaciones de la Sociedad Argentina de Antropología* 28, 153–165.

Garreaud, R. D. (2009). The andes climate and weather. *Adv. Geosci.* 22, 3–11. doi: 10.5194/adgeo-22-3-2009

Garrido, F. (2016). Rethinking imperial infrastructure: a bottom-up perspective on the Inca road. *J. Anthropol. Archaeol.* 43, 94–109. doi: 10.1016/j.jaa.2016.06.001

Gasco, A. (2018). Cazadores y pastores desde el 2000 AP en el límite sur del área Andina: estado de la cuestión y perspectivas futuras. *Cuadernos del Instituto Nacional de Antropología y Pensamiento Latinoamericano* 6, 15–38.

Genuer, R., Poggi, J.-M., and Tuleau-Malot, C. (2019). *VSURF Function | R Documentation*. Available online at: https://www.rdocumentation.org/packages/VSURF/versions/1.1.0/topics/VSURF [accessed July 14, 2020]

Giambiagi, L. B., Ramos, V. A., Godoy, E., Alvarez, P. P., and Orts, S. (2003). Cenozoic deformation and tectonic style of the andes, between 33\circ$ and 34\circ$ south latitude. *Tectonics* 22, n/a–n/a.

Giambiagi, L. B., Tunik, M., Ramos, V. A., and Godoy, E. (2009). The high andean cordillera of central argentina and chile along the piuquenes pass-cordon del portillo transect: darwin's pioneering observations compared eith modern geology. *Revista de la Asociación Geológica Argentina* 64, 43–54.

Gil, A. F., Villalba, R., Franchetti, F. R., Otaola, C., Abbona, C. C., Peralta, E. A., et al. (2020). Between foragers and farmers: climate change and human strategies in northwestern patagonia. *Quaternary* 3:17. doi: 10.3390/quat3020017

Gil, A. F., Villalba, R., Ugan, A., Cortegoso, V., Neme, G., Michieli, C. T., et al. (2014). Isotopic evidence on human bone for declining maize consumption during the little ice age in central western Argentina. *J. Archaeol. Sci.* 49, 213–227. doi: 10.1016/j.jas.2014.05.009

Goslee, S. C., and Urban, D. L. (2007). The ecodist package for dissimilarity-based analysis of ecological data. *J. Stat. Softw.* 22, 1–9.

Greenwell, B. M. (2017). Pdp: an r package for constructing partial dependence plots. *R J.* 9, 421–436 doi: 10.32614/rj-2017-016

Grimstead, D. N., Nugent, S., and Whipple, J. (2017). Why a standardization of strontium isotope baseline environmental data is needed and recommendations for methodology. *Adv. Archaeol. Pract.* 5, 184–195. doi: 10.1017/aap.2017.6

Hartmann, J., and Moosdorf, N. (2012). The new global lithological map database GLiM: a representation of rock properties at the Earth surface. *Geochem. Geophys. Geosyst.* 13:Q12004.

Hengl, T., de Jesus, J. M., Heuvelink, G. B. M., Gonzalez, M. R., Kilibarda, M., Blagotiæ, A., et al. (2017). SoilGrids250m: global gridded soil information based on machine learning. *PLoS One* 12:e0169748. doi: 10.1371/journal.pone.0169748

Jarvis, A., Reuter, A., Nelson, A., and Guevara, E. (2008). *Hole-Filled SRTM for the Globe Version 4*.

Jobbágy, E. G., Nosetto, M. D., Villagra, P. E., and Jackson, R. B. (2011). Water subsidies from mountains to deserts: their role in sustaining groundwater-fed oases in a sandy landscape. *Ecol. Appl.* 21, 678–694. doi: 10.1890/09-1427.1

Knudson, K. J., Goldstein, P. S., Dahlstedt, A., Somerville, A., and Schoeninger, M. J. (2014a). Paleomobility in the Tiwanaku diaspora: biogeochemical analyses at Rio Muerto. Moquegua Peru. *Am. J. Phys. Anthropol.* 155, 405–421. doi: 10.1002/ajpa.22584

Knudson, K. J., Pestle, W. J., Torres-Rouff, C., and Pimentel, G. (2012). Assessing the life history of an andean traveller through biogeochemistry: stable and radiogenic isotope analyses of archaeological human remains from Northern Chile. *Int. J. Osteoarchaeol.* 22, 435–451. doi: 10.1002/oa.1217

Knudson, K. J., Webb, E., White, C., and Longstaffe, F. J. (2014b). Baseline data for Andean paleomobility research: a radiogenic strontium isotope study of modern Peruvian agricultural soils. *Archaeol. Anthropol. Sci.* 6, 205–219. doi: 10.1007/s12520-013-0148-1

Kootker, L. M., van Lanen, R. J., Kars, H., and Davies, G. R. (2016). Strontium isoscapes in the Netherlands. spatial variations in 87Sr/86Sr as a proxy for palaeomobility. *J. Archaeol. Sci. Rep.* 6, 1–13. doi: 10.1016/j.jasrep.2016.01.015

Kuhn, M. (2013). *The Caret Package*. Available online at: http://topepo.github.io/caret/index.html [accessed July 14, 2020]

Kurtz, A. C., Kay, S. M., Charrier, R., and Farrar, E. (1997). Geochronology of Miocene plutons and exhumation history of the El Teniente region, Central Chile (34-35°8). *Andean Geol.* 24, 75–90.

Kutschera, W., and Müller, W. (2003). "Isotope language" of the Alpine Iceman investigated with AMS and MS. *Nucl. Instrum. Methods Phys. Res. B* 204, 705–719. doi: 10.1016/s0168-583x(03)00491-9

Kuznetsov, A. B., Semikhatov, M. A., and Gorokhov, I. M. (2012). The Sr isotope composition of the world ocean, marginal and inland seas: implications for the Sr isotope stratigraphy. *Stratigr. Geol. Correl.* 20, 501–515. doi: 10.1134/s0869593812060044

Laffoon, J. E., Sonnemann, T. F., Shafie, T., Hofman, C. L., Brandes, U., and Davies, G. R. (2017). Investigating human geographic origins using dual-isotope (87Sr/86Sr, δ18O) assignment approaches. *PLoS One* 12:e0172562. doi: 10.1371/journal.pone.0172562

Legendre, P., and Fortin, M. J. (1989). Spatial pattern and ecological analysis. *Vegetatio* 80, 107–138.

Llano, C. (2015). On optimal use of a patchy environment: archaeobotany in the Argentinean Andes (Argentina). *J. Archaeol. Sci.* 54, 182–192. doi: 10.1016/j.jas.2014.12.002

Llano, C., Cortegoso, V., and Marsh, E. (2017). Producción hortícola a baja escala en el límite continental del desarrollo andino: un aporte desde la arqueobotánica. *Darwiniana Nueva Serie* 5, 109–125. doi: 10.14522/darwiniana.2017.52.757

Mader, C., Hölzl, S., Heck, K., Reindel, M., and Isla, J. (2018). The llama's share: highland origins of camelids during the Late Paracas period (370 to 200 BCE) in south Peru demonstrated by strontium isotope analysis. *J. Archaeol. Sci. Rep.* 20, 257–270. doi: 10.1016/j.jasrep.2018.04.032

Mahowald, N. M., Muhs, D. R., Levis, S., Rasch, P. J., Yoshioka, M., Zender, C. S., et al. (2006). Change in atmospheric mineral aerosols in response to climate: last glacial period, preindustrial, modern, and doubled carbon dioxide climates: dust response to climate. *J. Geophys. Res.* 111, n/a–n/a.

Marsh, E. J. (2017). La fecha de la cerámica más temprana en los Andes sur. Una perspectiva macrorregional mediante modelos bayesianos. *Revista del Museo de Antropología Supl. Especial* 1, 83–94. doi: 10.31048/1852.4826.v10.n0.13501

Marsh, E. J., Kidd, R., Ogburn, D., and Durán, V. (2017). Dating the expansion of the inca empire: bayesian models from Ecuador and Argentina. *Radiocarbon* 59, 117–140. doi: 10.1017/rdc.2016.118

Masiokas, M. H., Rabatel, A., Rivera, A., Ruiz, L., Pitte, P., Ceballos, J. L., et al. (2020). A review of the current state and recent changes of the andean cryosphere. *Front. Earth Sci.* 8:99.

Méndez Melgar, C. (2013). Terminal pleistocene/early holocene 14C dates form archaeological sites in Chile: critical chronological issues for the initial peopling of the region. *Quat. Int.* 301, 60–73. doi: 10.1016/j.quaint.2012.04.003

Méndez, C., Nuevo Delaunay, A., Seguel, R., Maldonado, A., Murillo, I., Jackson, D., et al. (2018). Late pleistocene to early holocene high-quality quartz crystal procurement from the Valiente quarry workshop site (32°S, Chile, South America). *PLoS One* 13:e0208062. doi: 10.1371/journal.pone.0208062

Menéndez, L., Novellino, P., D'Addona, L. A., Brachetta Aporta, N., Béguelin, M., and Bernal, V. (2014). "El registro bioarqueológico y la incorporación de las prácticas agrícolas en el Centro– Norte de Mendoza," in *Arqueología de Ambientes de Altura de Mendoza y San Juan (Argentina)*, eds V. Cortegoso, V. A. Durán, and A. Gasco (Mendoza: EDIUNC), 99–123.

Miller, J. H., Crowley, B. E., Bataille, C. P., Wald, E. J., Kelly, A., Gaetano, M., et al. (2021). Historical landscape use of migratory caribou: new insights from old antlers. *Front. Ecol. Evol.* 8:590837.

Montgomery, J. (2010). Passports from the past: investigating human dispersals using strontium isotope analysis of tooth enamel. *Ann. Hum. Biol.* 37, 325–346. doi: 10.3109/03014461003649297

Montgomery, J., Evans, J. A., and Cooper, R. E. (2007). Resolving archaeological populations with Sr-isotope mixing models. *Appl. Geochem.* 22, 1502–1514. doi: 10.1016/j.apgeochem.2007.02.009

Muñoz-Schick, M., Moreira-Muñoz, A., Villagrán, C., and Luebert, F. (2000). Caracterización florística y pisos de vegetación en los Andes de Santiago, Chile Central. *Bol. Mus. Natl. Hist. Nat.* 49, 9–50.

Novellino, P. S., Aporta, N. B., D'Addona, L. A., Estrella, D., Bernal, V., Devincenzi, S., et al. (2013). Sitios de entierro de la localidad arqueológica Barrancas, Maipú (Mendoza, Argentina). *Intersec. Antropol.* 14, 271–277.

Ots, M. J., Garcia Llorca, J., and Cahiza, P. (2016). Recursos y estrategias de consumo en el Centro de Mendoza entre los siglos X-XVI AD. *Intersecciones en Antropología* 17, 375–387.

Oyarzabal, M., Clavijo, J., Oakley, L., Biganzoli, F., Tognetti, P., Barberis, I., et al. (2018). Unidades de vegetación de la Argentina. *Ecol. Austral* 28, 040–063.

Pavlovic, D., Sánchez, R., Pascual, D., Martínez, A., and Cortés, C. (2019). Rituales de la vida y de la muerte: dinámicas de interacción entre el Tawantinsuyu y las poblaciones locales en la cuenca del Maipo-Mapocho. *Chile Central. Estud. Atacameños.* 63, 43–80. doi: 10.2307/j.ctvf3w3k5.6

Pin, C., Briot, D., Bassin, C., and Poitrasson, F. (1994). Concominant separation of strontium and samarium–neodymium for isotopic analysis in silicate samples, based on specific extraction chromatography. *Analytica Chimica Acta* 298, 209–217. doi: 10.1016/0003-2670(94)00274-6

Planella, M. T., Falabella, F., Belmar, C., and Quiroz, L. (2015). Huertos, chacras y sementeras. *Plantas cultivadas* y su participación en los desarrollos culturales de Chile central. *Rev. Esp. Antropol. Am.* 44, 495–522.

Price, T. D., Burton, J. H., and Bentley, R. A. (2002). The characterization of biologically available strontium isotope ratios for the study of

prehistoric migration. *Archaeometry* 44, 117–135. doi: 10.1111/1475-4754.00047

Price, T. D., Manzanilla, L., and Middleton, W. D. (2000). Immigration and the ancient city of teotihuacan in mexico: a study using strontium isotope ratios in human bone and teeth. *J. Archaeol. Sci.* 27, 903–913. doi: 10.1006/jasc.1999.0504

Probst, P., Wright, M. N., and Boulesteix, A.-L. (2019). Hyperparameters and tuning strategies for random forest. *WIREs Data Min. Knowl. Discov.* 9:e1301.

R Core Team (2020). *R: a Language and Environment for Statistical Computing*. Vienna: R Foundation for Statistical Computing.

Ramos, V. A., and Folguera, A. (2009). Andean flat-slab subduction through time. *Geol. Soc. London Spec. Publ.* 327, 31–54. doi: 10.1144/sp327.3

Reynolds, A. C., Quade, J., and Betancourt, J. L. (2012). Strontium isotopes and nutrient sourcing in a semi-arid woodland. *Geoderma* 18, 574–584. doi: 10.1016/j.geoderma.2012.06.029

Rusconi, C. (1962). *Poblaciones Pre y Post Hispánicas de Mendoza. Arqueología*, Vol. III. Mendoza.

Sanhueza, L., and Falabella, F. (1999). Las comunidades alfareras iniciales en Chile central. *Revista Chilena de Antropología* 15, 29–47.

Santana-Sagredo, F., Schulting, R. J., Méndez-Quiros, P., Vidal-Elgueta, A., Uribe, M., Loyola, R., et al. (2021). White gold' guano fertilizer drove agricultural intensification in the Atacama desert from ad 1000. *Nature Plants* 7, 152–158

Scaffidi, B. K., and Knudson, K. J. (2020). An archaeological strontium isoscape for the prehistoric andes: understanding population mobility through a geostatistical meta-analysis of archaeological 87Sr/86Sr values from humans, animals, and artifacts. *J. Archaeol. Sci.* 117:105121. doi: 10.1016/j.jas.2020.105121

Scaffidi, B. K., Tung, T. A., Gordon, G., Alaica, A. K., González, La Rosa, L. M., et al. (2020). Drinking locally: a water 87Sr/86Sr isoscape for geolocation of archeological samples in the peruvian andes. *Front. Ecol. Evol.* 8:281.

Scott, M., le Roux, P., Sealy, J., and Pickering, R. (2020). Lead and strontium isotopes as palaeodietary indicators in the Western Cape of South Africa. *S. Afr. J. Sci.* 116, 1–8. doi: 10.15700/saje.v38ns2a1416

Serna, A., Prates, L., Mange, E., Salazar-García, D. C., and Bataille, C. P. (2020). Implications for paleomobility studies of the effects of quaternary volcanism on bioavailable strontium: a test case in North Patagonia (Argentina). *J. Archaeol. Sci.* 121:105198. doi: 10.1016/j.jas.2020.105198

Serna, A., Prates, L., Valenzuela, L. O., and Salazar-García, D. C. (2019). Back to the bases: building a terrestrial water δ18O baseline for archaeological studies in North Patagonia (Argentina). *Quat. Int.* 548, 4–12. doi: 10.1016/j.quaint.2019.06.008

Slovak, N. M., Paytan, A., Rick, J. W., and Chien, C.-T. (2018). Establishing radiogenic strontium isotope signatures for Chavín de Huántar, Peru. *J. Archaeol. Sci. Rep.* 19, 411–419. doi: 10.1016/j.jasrep.2018.03.014

Snoeck, C., Pouncett, J., Claeys, P., Goderis, S., Mattielli, N., Parker Pearson, M., et al. (2018). Strontium isotope analysis on cremated human remains from stonehenge support links with west wales. *Sci. Rep.* 8:10790.

Snoeck, C., Ryan, S., Pouncett, J., Pellegrini, M., Claeys, P., Wainwright, A. N., et al. (2020). Towards a biologically available strontium isotope baseline for Ireland. *Sci. Total Environ.* 712:136248. doi: 10.1016/j.scitotenv.2019.136248

Standen, V. G., Santoro, C. M., Arriaza, B., and Coleman, D. (2018). Hunting, gathering, and fishing on the coast of the atacama desert: chinchorro population mobility patterns inferred from strontium isotopes. *Geoarchaeology* 33, 162–176. doi: 10.1002/gea.21594

Takigami, M., Uzawa, K., Seki, Y., Chocano, D. M., and Yoneda, M. (2019). Isotopic evidence for camelid husbandry during the formative period at the pacopampa site, peru. *Environ. Archaeol.* 25, 262–278. doi: 10.1080/14614103.2019.1586091

Thomsen, E., and Andreasen, R. (2019). Agricultural lime disturbs natural strontium isotope variations: implications for provenance and migration studies. *Sci. Adv.* 5:eaav8083. doi: 10.1126/sciadv.aav8083

Tipple, B. J., Valenzuela, L. O., and Ehleringer, J. R. (2018). Strontium isotope ratios of human hair record intra-city variations in tap water source. *Sci .Rep.* 8:3334.

Torres-Rouff, C., and Knudson, K. J. (2017). Integrating identities: an innovative bioarchaeological and biogeochemical approach to analyzing the multiplicity of identities in the mortuary record. *Curr. Anthropol.* 58, 381–409. doi: 10.1086/692026

Troncoso, A. (2018). "Inca landscapes of domination," in *The Oxford Handbook of the Incas*, eds S. Alconini and A. Covey (Oxfort: Oxford University Press).

Ugan, A., Neme, G., Gil, A., Coltrain, J., Tykot, R., and Novellino, P. (2012). Geographic variation in bone carbonate and water δ18O values in Mendoza, Argentina and their relationship to prehistoric economy and settlement. *J. Archaeol. Sci.* 39, 2752–2763. doi: 10.1016/j.jas.2012.04.013

Willmes, M., Bataille, C. P., James, H. F., Moffat, I., McMorrow, L., Kinsley, L., et al. (2018). Mapping of bioavailable strontium isotope ratios in France for archaeological provenance studies. *Appl. Geochem.* 90, 75–86. doi: 10.1016/j.apgeochem.2017.12.025

Wright, M. N., and Ziegler, A. (2017). Ranger: a fast implementation of random forests for high dimensional data in C++ and R. *J. Statist. Softw.* 77, 1–17. doi: 10.18637/jss.v077.i01

Yu, H., Spyrou, M. A., Karapetian, M., Shnaider, S., Radzevičiūtė, R., and Nägele, K. (2020). Paleolithic to bronze age siberians reveal connections with first americans and across Eurasia. *Cell* 181, 1232–1245.e20.

Conflict of Interest: The authors declare that the research was conducted in the absence of any commercial or financial relationships that could be construed as a potential conflict of interest.